Transportation Consortium of South-Central States

Tran-SET

Solving Emerging Transportation Resiliency, Sustainability, and Economic Challenges through the Use of Innovative Materials and Construction Methods: From Research to Implementation

Structural Vulnerability of Coastal Bridges Under Extreme Hurricane Conditions

Project No. 18STTSA04

Lead University: University of Texas at San Antonio

Final Report

August 2019

Disclaimer

TECHNICAL DOCUMENTATION PAGE

1. Project No.	2. Government Accession No.	3. Recipient's Catalog No.
18STTSA04		

4. Title and Subtitle	5. Report Date
Structural Vulnerability of Coastal Bridges Under Extreme Hurricane Conditions	Aug. 2019
	6. Performing Organization Code
7. Author(s)	**8. Performing Organization Report No.**
PI: Arturo Montoya https://orcid.org/0000-0003-1429-5105 Co-PI: Adolfo Matamoros https://orcid.org/0000-0002-5312-7764 Co-PI: Firat Testik https://orcid.org/0000-0002-1259-0162 GRA: Reza Nasouri https://orcid.org/0000-0001-7232-9372 GRA: Adnan Shahriar https://orcid.org/0000-0002-2903-4859 GRA: Arsalan Majlesi https://orcid.org/0000-0001-5514-1562	
9. Performing Organization Name and Address	**10. Work Unit No. (TRAIS)**
Transportation Consortium of South-Central States (Tran-SET) University Transportation Center for Region 6 3319 Patrick F. Taylor Hall, Louisiana State University, Baton Rouge, LA 70803	**11. Contract or Grant No.** 69A3551747106
12. Sponsoring Agency Name and Address	**13. Type of Report and Period Covered**
United States of America Department of Transportation Research and Innovative Technology Administration	Final Research Report Mar. 2018 – Mar. 2019
	14. Sponsoring Agency Code

15. Supplementary Notes

Report uploaded and accessible at [Tran-SET's website (http://transet.lsu.edu/)](http://transet.lsu.edu/).

16. Abstract

This work presents the results of a numerical study evaluating the response of coastal bridges due to hurricane-induced waves. The analyses were conducted using the Coupled Eulerian-Lagrangian (CEL) approach, available on the commercial finite element software Abaqus, which allows modeling the interaction between water and the bridge. The work concentrated on (1) establishing an approach for modeling the desired wave characteristics (i.e., wave height, and frequency) within the CEL simulation, (2) conducting simulations using actual bridge dimensions of historically damaged bridges, (3) analyzing a range of foundation flexibilities to determine its effect on the uplift and shear forces acting on the superstructure, and (4) comparing results simulations to AASHTO equations that estimate wave forces acting on coastal bridges. The numerical study revolved around two major highway bridges damaged along the U.S Gulf Coast during hurricane Katrina in 2005, (a) the U.S 90 highway bridge over Biloxi Bay and (b) the US. 90 St. Louis-Bay Bridge. The water level elevation was defined at the bottom of the superstructure as post-Katrina investigations revealed that this was a common characteristic for damaged bridges. The analysis revealed that (a) bridge models with flexible foundations provide better force design estimates than models with rigid supports, (b) the force demands are presumably amplified when the natural frequency of the bridge coincides with that of the traveling waves, and (c) CEL force estimates show large peak magnitudes during wave impacts that exceed AASHTO estimates. Further research is required to determine if these peaks are numerical artifacts or a concern for connection design.

17. Key Words	18. Distribution Statement
Bridge, Hurricane, Resiliency, Failure, Waves	No restrictions. This document is available through the National Technical Information Service, Springfield, VA 22161.

19. Security Classif. (of this report)	20. Security Classif. (of this page)	21. No. of Pages	22. Price
Unclassified	Unclassified	37	

Form DOT F 1700.7 (8-72) **Reproduction of completed page authorized.**

SI* (MODERN METRIC) CONVERSION FACTORS

APPROXIMATE CONVERSIONS TO SI UNITS

Symbol	When You Know	Multiply By	To Find	Symbol
		LENGTH		
in	inches	25.4	millimeters	mm
ft	feet	0.305	meters	m
yd	yards	0.914	meters	m
mi	miles	1.61	kilometers	km
		AREA		
in^2	square inches	645.2	square millimeters	mm^2
ft^2	square feet	0.093	square meters	m^2
yd^2	square yard	0.836	square meters	m^2
ac	acres	0.405	hectares	ha
mi^2	square miles	2.59	square kilometers	km^2
		VOLUME		
fl oz	fluid ounces	29.57	milliliters	mL
gal	gallons	3.785	liters	L
ft^3	cubic feet	0.028	cubic meters	m^3
yd^3	cubic yards	0.765	cubic meters	m^3
		NOTE: volumes greater than 1000 L shall be shown in m^3		
		MASS		
oz	ounces	28.35	grams	g
lb	pounds	0.454	kilograms	kg
T	short tons (2000 lb)	0.907	megagrams (or "metric ton")	Mg (or "t")
		TEMPERATURE (exact degrees)		
^oF	Fahrenheit	5 (F-32)/9 or (F-32)/1.8	Celsius	^oC
		ILLUMINATION		
fc	foot-candles	10.76	lux	lx
fl	foot-Lamberts	3.426	candela/m^2	cd/m^2
		FORCE and PRESSURE or STRESS		
lbf	poundforce	4.45	newtons	N
lbf/in^2	poundforce per square inch	6.89	kilopascals	kPa

APPROXIMATE CONVERSIONS FROM SI UNITS

Symbol	When You Know	Multiply By	To Find	Symbol
		LENGTH		
mm	millimeters	0.039	inches	in
m	meters	3.28	feet	ft
m	meters	1.09	yards	yd
km	kilometers	0.621	miles	mi
		AREA		
mm^2	square millimeters	0.0016	square inches	in^2
m^2	square meters	10.764	square feet	ft^2
m^2	square meters	1.195	square yards	yd^2
ha	hectares	2.47	acres	ac
km^2	square kilometers	0.386	square miles	mi^2
		VOLUME		
mL	milliliters	0.034	fluid ounces	fl oz
L	liters	0.264	gallons	gal
m^3	cubic meters	35.314	cubic feet	ft^3
m^3	cubic meters	1.307	cubic yards	yd^3
		MASS		
g	grams	0.035	ounces	oz
kg	kilograms	2.202	pounds	lb
Mg (or "t")	megagrams (or "metric ton")	1.103	short tons (2000 lb)	T
		TEMPERATURE (exact degrees)		
^oC	Celsius	1.8C+32	Fahrenheit	^oF
		ILLUMINATION		
lx	lux	0.0929	foot-candles	fc
cd/m^2	candela/m^2	0.2919	foot-Lamberts	fl
		FORCE and PRESSURE or STRESS		
N	newtons	0.225	poundforce	lbf
kPa	kilopascals	0.145	poundforce per square inch	lbf/in^2

TABLE OF CONTENTS

TECHNICAL DOCUMENTATION PAGE ii
TABLE OF CONTENTS iv
LIST OF FIGURES v
LIST OF TABLES vii
ACRONYMS, ABBREVIATIONS, AND SYMBOLS viii
EXECUTIVE SUMMARY ix
1. INTRODUCTION 1
2. OBJECTIVES 3
3. LITERATURE REVIEW 4
3.1. AASHTO Guide Specification for Bridges Vulnerable to Coastal Storms 6
3.2. Douglass Equations 8
4. METHODOLOGY 10
4.1. Numerical Approach 10
4.1.1. Background Theory 10
4.1.2. Wave Generation 11
4.1.3. Three-Dimensional Effect 14
4.2. Model Development for Wave Generation 16
4.3. Bridge Models 24
4.4. Parametric Study 27
4.4.1. Flexibility of the Substructure 27
4.4.2. Variation in the Boundary Conditions 28
5. ANALYSIS AND FINDINGS 30
5.1. Rigid Support System 30
5.2. Flexible Support System 33
5.3. One Pier Model 34
6. CONCLUSIONS 37
REFERENCES 38
APPENDIX A: US-90 BRIDGE OVER BAY ST. LOUIS DRAWINGS 40

LIST OF FIGURES

Figure 1. Variables involved in the AASHTO equations, after *(5)*. 6

Figure 2. Maximum vertical force and associated forces, after *(5)*. 7

Figure 3. Maximum horizontal force and associated forces, after *(5)*. 8

Figure 4. Numerical wave generation schematic. 12

Figure 5. ABAQUS velocity input. 12

Figure 6. Periodic wave schematic. 13

Figure 7. Mesh of a thick and thin domain with equivalent initial conditions. 15

Figure 8. Initial water (indicated in blue) and voids (indicated in red) regions of the simulation. 15

Figure 9. Water condition at t=4.5 s. 15

Figure 10. Maximum wave height vs. time. 16

Figure 11. Velocity profile at boundary condition... 17

Figure 12. Free surface elevation at time 30 s. 17

Figure 13. Model Partition (Zoom at the 50 m portion from right edge). 18

Figure 14. Boundary conditions... 18

Figure 15. Meshing with initial water (zoomed at the 50 m portion from the right edge). 19

Figure 16. 3D simulation domain. 20

Figure 17. Wave profile for t=3 s to t=15 s. 21

Figure 18. Wave profile for t=18 s to t=30 s. 21

Figure 19. Velocity magnitude profile at time=30 s. 22

Figure 20. Free surface elevation vs. time vs. space. 23

Figure 21. Free surface profile at x=39 m. 23

Figure 22. Mesh sensitivity analysis. 24

Figure 23. Deck Configuration for the I-10 Biloxi-Bay Bridge. 25

Figure 24. Deck Configuration for the US-90 St. Louis-Bay Bridge. 26

Figure 25. CEL simulations domain: Green domain is Lagrangian, Blue (water) and Gray (initial voids) are Eulerian. 27

Figure 26. Biloxi-Bay Bridge model with flexible substructure conditions. 28

Figure 27. Pier length dimensions and water elevation for the models with flexible substructure conditions. 28

Figure 28. Configuration of the Biloxi-Bay Bridge. 29
Figure 29. Biloxi-Bay bridge model within the fluid domain. 29
Figure 30. Wave impact sequence on St. Louis and Biloxi-Bay bridge with rigid supports. 30
Figure 31. Elevation view of wave impact sequence on St. Louis and Biloxi-Bay bridge with rigid supports. 31
Figure 32. Normalized Uplift and shear force on front deck. 32
Figure 33. Normalized Uplift and shear force on rear deck. 32
Figure 34. Normalized uplift and shear force on rear deck. 33
Figure 35. Uplift forces for different height of piers. 34
Figure 36. Shear forces for different height of piers. 34
Figure 37. Uplift Force-Front deck of one pier model. 35
Figure 38. Shear Force-Front deck of one pier model. 35
Figure 39. Uplift Force-Rear deck of one pier model. 36
Figure 40. Uplift Force-Rear deck of one pier model. 36

LIST OF TABLES

Table 1. Input parameters used to generate the velocity wave profile in ABAQUS. 16

Table 2. Wave properties generated using the analytical method. 16

Table 3. Domains defined in the ABAQUS model... 18

Table 4. Dimensions and configurations of the I-10 and U.S 90 bridges. 25

ACRONYMS, ABBREVIATIONS, AND SYMBOLS

AASHTO	American Association of State Highway and Transportation Officials
CEL	Coupled Eulerian-Lagrangian
CFD	Computational Fluid Dynamics
C-IEPM	Epoxy-Polyurea Matrix
DOT	Department of Transportation
FEM	Finite Element Method
FSI	Fluid Structure interaction
NOAA	National Oceanic and Atmospheric Administration
OSU	Oregon State University
SIFUM	Solver for Incompressible Flow on Unstructured Mesh
SPH	Smoothed Particle Hydrodynamics
UTSA	University of Texas at San Antonio

EXECUTIVE SUMMARY

The frequency and intensity of recent hurricanes have urged the need of taking proactive actions that prevent future hurricane damages to coastal bridges. A crucial step towards addressing this need is to accurately quantify the vulnerability of coastal infrastructure to extreme hurricane storms. Engineers can prevent failures of coastal bridges during extreme hurricanes by ensuring that wave-induces forces do not exceed the structural capacity of bridges.

The main objective of this study is to provide and analysis technique that can be used in designing structural modifications to coastal bridges that mitigate damages in the events of extreme hurricanes and storm surges. Finite element-based approaches are attractive in the simulation of wave impacts on bridges during a hurricane event because of their ability to provide a comprehensive and holistic assessment of the deformations and stresses experienced by the bridge. In a previous report by the UTSA research team, it has been concluded that Coupled Eulerian-Lagrangian (CEL) method, is a well-suited technique for predicting the behavior of coastal bridges under hurricane-induced waves.

The work of this study was focused on (1) establishing an approach for modeling the desired wave characteristics (i.e., wave height, and frequency) within the CEL simulations, (2) conducting numerical simulations using actual bridge dimensions of historically damaged bridges rather than conducting simulations on scale models as encountered in literature, (3) analyzing a range of foundation flexibilities to determine its effect on the uplift and shear forces acting on the superstructure, and (4) comparing results simulations to AASHTO force demand equations provided in the Guide Specification for Bridges Vulnerable to Coastal Storms. AASHTO equations provide a single force magnitude for the shear and the uplift force, which represents the maximum force that the superstructure must resist.

The analysis revolved around two major highway bridges along the U.S. Gulf Coast that were severely damaged during hurricane Katrina in 2005, (a) the U.S 90 highway bridge over Biloxi-Bay and (b) the U.S 90 St. Louis-Bay Bridge. The wave characteristics of the simulation were defined according to the records of catastrophic hurricanes in the Gulf Coast. The impact of the flexibility of the substructure configuration on the bridge behavior was evaluated by varying the pier lengths of the bridge models.

The numerical analyses conducted in this study confirmed that the CEL technique is an efficient numerical approach for elucidating the hydrodynamic behavior of coastal bridges under storm surge and hurricane wave loads. The stresses at the interface between the superstructure and substructure were integrated over the interface area in order to determine the history profile of the uplift and shear forces acting on the superstructure. The comparison of CEL results to AASHTO equations provided a means to establish confidence on the numerical analysis, but also raised some concerns to be clarified in future research studies. Overall, the simulation's uplift and shear force estimates were in the range of AASHTO estimates but exhibited large numerical peaks that exceeded the magnitude of the AASHTO equations. These peaks coincided with the instances in which the wave impacted the superstructure, i.e., a pulse-type loading. Further work is required to determine if these peaks are numerical artifacts or a concern for connection design. Moreover, the flexibility of the substructure was shown to influence the bridge force demands. These forces are presumably amplified when the natural period of the bridge coincides with that of the traveling waves.

1. INTRODUCTION

Coastal bridges are prone to failure during extreme hurricane events. However, the strategies adopted to cope with this natural hazard in the United States have been reactive rather than proactive. During hurricanes Ivan (September 2004) and Katrina (August 2005), major highway bridges were damaged along the U.S Gulf Coast. Padgett et al. *(1)* indicated that the cost of repairing and replacing bridges damaged during hurricane Katrina exceeded 1 billion dollars. The most severe damage consisted of superstructure collapse due unseating of the deck, caused by the combined actions of storm surge and hydrodynamic forces from waves. Major damaged bridges shared some similar characteristics, including: (a) noncontinuous concrete spans, (b) inadequate or nonexistent connections between superstructure and bent caps, and (c) storm surge elevation approaching or exceeding the elevation of the bottom span. According to post-disaster surveys, the performance of the connections between the superstructure and substructure can determine the survivability of the bridge superstructure during hurricane events. For some coastal bridges, shear keys were sufficient to prevent unseating of the superstructure.

While reactive actions are necessary after extreme weather events, the frequency and intensity of recent hurricanes, such as Harvey (August 2017), Irma (September 2017), and Maria (September 2017), have demonstrated the need of taking proactive actions to prevent major damages. A crucial step toward addressing this need is to accurately quantify the vulnerability of coastal infrastructure to extreme hurricane storms. Engineers can prevent failures of coastal bridges during extreme hurricanes by ensuring that wave-induces forces do not exceed the structural capacity of the bridge. This safety check requires accurately estimating the hydrodynamic forces acting on the bridge structure during a hurricane.

Finite element-based approaches are attractive for simulating wave impacts on bridges during a hurricane event because of their ability to provide a comprehensive and holistic assessment of the deformations and stresses experienced by the bridge, which cannot be obtained from simple analytical equations or by simplifying the wave-induced loading. In a former study *(2)*, the authors researched available techniques for modeling Fluid-Structure Interaction (FSI) and tested the accuracy and efficiency of two numerical techniques, the Smooth Particle Hydrodynamics (SPH) and Coupled Eulerian-Lagrangian (CEL) method, in simulating the response of bridge structures due to wave loads. After testing both analysis techniques, it was concluded that the CEL platform is better suited for the proposed application.

In the CEL technique, solids are simulated with Lagrangian meshes, while fluids are simulated using Eulerian meshes. Lagrangian meshes are attached to material points, and as the materials deform, the mesh deforms with them. Eulerian meshes remain the same as the material flows (or deforms) within the mesh, acting as a background grid *(3)*. CEL allows the definition of inlet and outlet boundary conditions that are required to simulate the wave flow conditions. Although CEL simulations are computational costly, they provide a full description of the stress field acting on the bridge members.

CEL simulations can increase the understanding of the behavior of coastal bridges during extreme hurricane events. This understanding will lead to identifying bridge structures that are more resilient to hurricane waves and storm surge. The conclusions and modeling framework obtained from this study can be used by bridge authorities in the Texas-Louisiana coastline to make informed decisions for preserving the structural integrity of a large coastal bridge network, while making the optimum use of the resources allocated for this purpose. Moreover, recent extreme hurricane events have shown that design procedures should consider scenarios that exceed historical records. New design configurations should be developed to minimize the structural damage during an extreme hurricane event, e.g. connections that prevent unseating of the superstructure.

2. OBJECTIVES

The objective of this study is to provide and analysis technique that can be used in designing structural modifications to coastal bridges that mitigate damages in the events of extreme hurricanes and storm surges. Properly validated and calibrated high-fidelity models can be used to identify bridge configurations (i.e., geometric configuration of the superstructure) and types of bridge supports that are most susceptible to severe damage under the occurrence of extreme hurricanes and storm surge events. The current study is a proof-of-concept to validate the use of the proposed numerical method, Coupled Eulerian-Lagrangian Analysis technique, for evaluating structural modifications that can be incorporated into current and future bridges to minimize damages during extreme hurricanes and storm surges.

3. LITERATURE REVIEW

In a preceding report, the authors summarized the different numerical analysis techniques that are used to model fluid–structure interaction *(2)*. The reader is referred to the aforementioned report for a comprehensive review of the simulation techniques that have been used for the study of FSI problems related to wave impact on bridges. The current literature review focuses on the latest research studies in this field in the past few years. The continuous research trend in this research field is to conduct experiments and numerical simulations on scale model bridges to determine the wave forces acting on coastal bridges, both through theoretical and empirical models. Based on the literature review, it was concluded that previous work and post-disaster recovery investigations have highlighted:

- the importance of strengthening the connection between the superstructure and substructure in order to prevent shifting or unseating of the superstructure during an extreme hurricane event,
- the importance of defining a critical deck elevation in order to minimize the probability of failure,
- the importance of considering different types of wave conditions in the numerical simulations to improve the accuracy of the estimated force demands, and
- the importance of comparing numerical results with different approaches in order to establish confidence on the generated results.

Relevant literature expanding on the four items listed above is provided below.

Hayatdavoodi et al. *(4)* studied nonlinear periodic and solitary wave loads on submerged, horizontal decks in shallow water. The loads were determined using level I Green-Naghdi (GN) equations. A parametric study was performed in which the wave height, wave period, deck submergence depth and deck length, were varied to determine their influence on the horizontal and vertical wave-induced loads and the overturning moment. The results of the parametric study were used to develop empirical relations that estimate the wave loads on submerged decks. Due to the assumption of the GN equations, the effects of air entrapment or wave breaking were not considered in the empirical equations. The equations were used to estimate the demand forces on the decks of Punaluu Bridge and Maipalaoa Bridge in Hawaii, USA. The results of the empirical equations were reported to be in good agreement with OPENFOAM results; however, they were found to overestimate the Computational Fluid Dynamics (CFD) results. AASHTO *(5)* equations were found to overestimate the calculations by a factor of 10 for the Puanluu Bridge, but to underestimate the horizontal forces in the Maipalaoa Bridge.
Park et al. *(6)* compared the results provided by two CFD model packages, IHFOAM and ANSYS-FLUENT, for the wave-induced force on an elevated structure. The model validation consisted of comparing the pressure and forces computed numerically against those obtained experimentally on a 1:10 physical model. Three regular wave conditions were generated: (a) non-breaking, (b) breaking, and (c) broken. The analysis revealed that the agreement between IHFOAM and FLUENT was dependent on the wave conditions. The methods were in best agreement for non-breaking conditions, while exhibited poor agreement for the broken conditions.

Saeidpour et al. *(7)* proposed a computationally efficient methodology for developing structural fragility curves of simply supported coastal bridges vulnerable to hurricane hazard. The intensity of the hurricane hazard is quantified in terms of the wind speed as it is assumed to control the surge height and wave characteristics. The uniqueness of the proposed method includes the consideration of uncertainties in extreme wave heights and wave period by means of a wave spectral density distribution in the calculation of wave forces. The proposed hurricane risk analysis method was applied to analyze coastal bridges in the state of Georgia. The study showed a negative correlation between deck elevation and risk of failure, emphasizing the importance of providing sufficient deck elevation in the design of coastal bridges.

Yuan et al. *(8)* focused on studying the connection, or interface, between the bridge superstructure and substructure. They presented a three step framework for evaluating the bridge deck-wave interaction, which first consists of determining the storm surge or wave that can be generated at a site, then predicting the wave forces generated due to the storm surge and wave information, and finally, determining the structural capacity of the bridge. A finite element model that determines the capacity of a clip-bolt-type connection, typically used to connect prestressed concrete girders and bent caps, was proposed and verified with an experimental study. The FEM model was used to determine the ultimate resistance envelope of the connection. Yuan et al. clarified that the critical elevation below which the spans are expected to be shifted is a function of many variables, including (a) self-weight of the bridge span, (b) connection type and capacity, and (c) storm surge and wave forces, (d) and bridge elevation.

He et al. *(9)* proposed a new Carbon-fiber Interfacial Epoxy-Polyurea Matrix (C-IEPM) composite to strengthen the connection detail of coastal bridges. The effectiveness of IEPM effectiveness was demonstrated by testing six scaled concrete girders using a modified simulated storm surge and slamming wave force function. The two girders that were designed using AASHTO *(5)* field connection-details exhibited concrete shear failure in less than one-half load cycle. Conventional fiber reinforced strengthened girders failed in less than one load cycle, experiencing severe damage on its girder-to-cap connection. On the other hand, the C-IEPM-strengthened girder only experienced local cracking after 12 cycles.

Huang et al. *(10)* conducted experimental and numerical modeling to determine the hurricane induced wave forces on a box girder deck of a coastal bridge. The experiments were conducted on 1:30 scale model in a wave flume under different wave conditions and various submerged and elevated conditions. Two dimensional numerical simulations were run in OpenFOAM, open source CFD platform. Numerical simulations were performed on a T-type girder deck with similar dimension as the box girder deck and under the same wave loading conditions. The difference in the results showed that the interactions of the wave with these two girders led to significant differences. As most empirical formulations have been established for T-type girder decks, Huang et al. *(10)* proposed a new formulation for estimating the maximum wave forces on box girder superstructures.

Qu et al. *(11)* conducted a numerical investigation on the effect of considering the joint action of solitary waves and currents on the hydrodynamic loads acting on a bridge deck. The waves and currents were simulated using the Solver for Incompressible Flow on Unstructured Mesh (SIFUM). The results of the study indicated that current in the wave direction leads to a higher maximum of the hydrodynamic force in the horizontal direction, and a current in the opposite direction results in a lower maximum. The submersion depth was found to influence the vertical component of hydrodynamic load when a current is present. It was also observed that the maximum horizontal and vertical components of hydrodynamic loads increased linearly with wave height and decreased as water depth increased. Lastly, currents were found to influence the efficiency of the air vents, either position or negative, in reducing the hydrodynamic loads.

3.1. AASHTO Guide Specification for Bridges Vulnerable to Coastal Storms

AASHTO *(5)* developed guidelines for estimating the hydrostatic and hydrodynamic forces and moments acting on superstructures of coastal bridges. These equations were derived based on a Physics Based Model (PBM) developed for estimating wave forces on offshore platforms. AASHTO's commentaries acknowledges that offshore platforms' geometrical and wave characteristics are significantly different that those of coastal bridges. Platforms decks are thin horizontal structures located in deep open waters, while bridge structures have finite thicknesses and are in shallow waters. The PBM equations developed for coastal bridges have the same general format as those of the offshore platforms, but their derivation varied in the way that they were applied to the structure.

The computation of the design forces requires knowledge of the water depths and the wave conditions of the actual storm striking the bridge of interest during the past 100 years. In addition, geometric information of the superstructure information is needed, including the span lengths, span widths, deck thickness, beam type, number of beams, overhang, rail height and bed elevation at each span. Another relevant variable for evaluating AASHTO equations is the clearance, which measures the distance between the storm water level and the low chord elevation. For the case where the storm water level is below the deck of the bridge, the clearance is positive. Conversely, for the case where the storm water level is above the bottom of the deck, the clearance is negative. Water depth is the distance between the storm water level and the bed elevation.

AASHTO equations were used by Sheppard et al. *(12)* to analyze over 500 bridge spans in Louisiana to better understand the vulnerability of these bridges to design storm surge and wave loads. The study identified several bridge spans across Louisiana that were susceptible to serious damages. As part of this work, they coded AASHTO equations on a Wave Load Calculation Program. This program was used to obtain reference design loads in the current study.

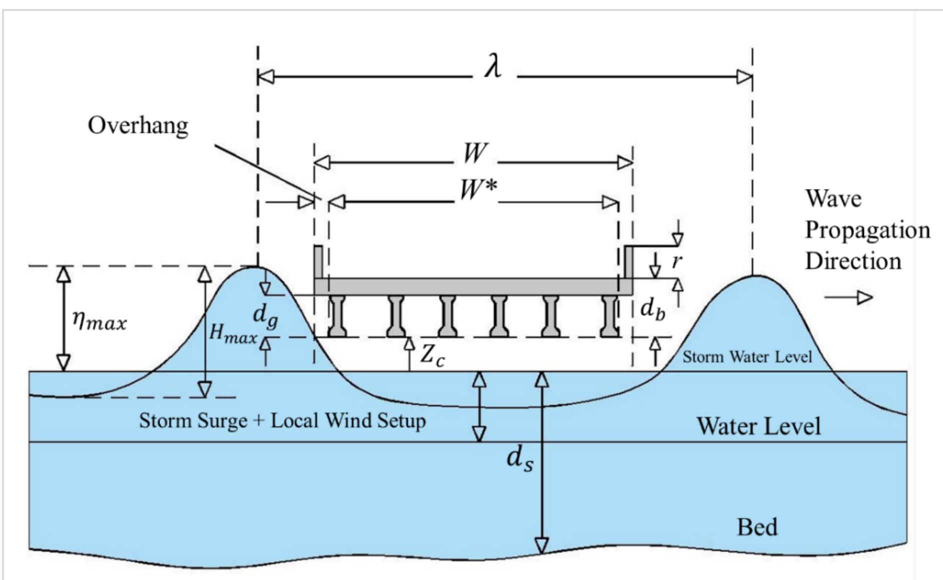

Figure 1. Variables involved in the AASHTO equations, after *(5)*.

The variables shown in Figure 1 are described as below:

H_{max}: Max wave height;
λ: Wavelength;
T_p: Period of waves with the greatest energy exhibited in a spectrum;
η_{max}: Wave crest height above storm water level;
d_s: Storm water depth at the bridge;
d_b: Girder height and deck thickness;
d_g: Girder height;
r: Rail height; and
W: Deck width.

Once these variables are known, two force cases on the superstructure should be calculated. Case 1 computes the maximum vertical force, $F_{V\text{-}MAX}$, and the associated horizontal force, $F_{H\text{-}AV}$, moment, $M_{T\text{-}AV}$, and the vertical slamming force, F_S, as illustrated in Figure 2. Coefficients for computing $F_{V\text{-}MAX}$ vary according to the span type, girder span versus slab span; while coefficients for computing $F_{H\text{-}AV}$ vary per girder type. Case 1 is used to design the vertical resistance to prevent the superstructure from unseating. Case 2 computes the maximum horizontal force, $F_{H\text{-}MAX}$ and the associated horizontal force, $F_{V\text{-}AH}$, moment, $M_{T\text{-}AH}$, and the vertical slamming force, F_S, as illustrated in Figure 3. Case 2 is used to design the horizontal resistance of piers and horizontal restraints, e.g. shear keys.

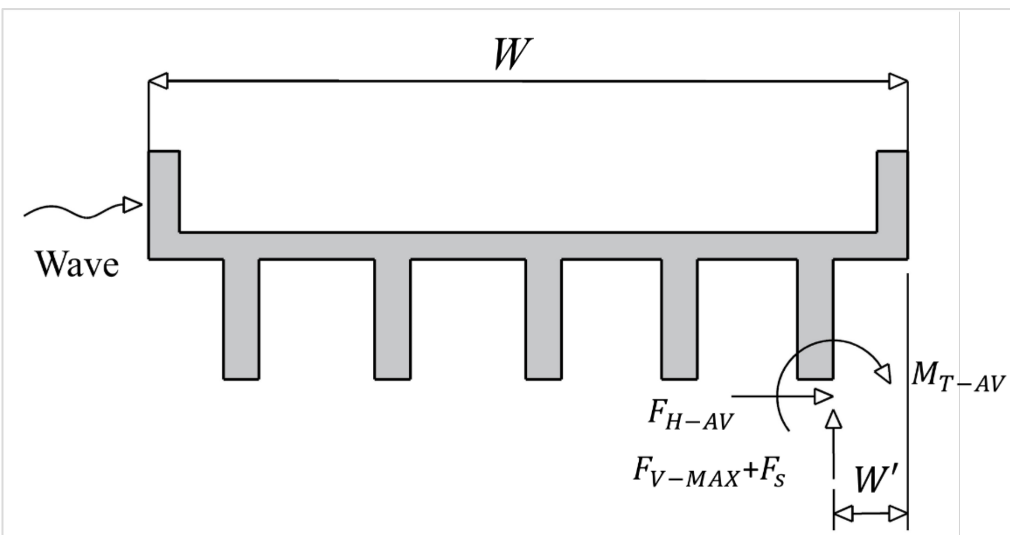

Figure 2. Maximum vertical force and associated forces, after *(5)*.

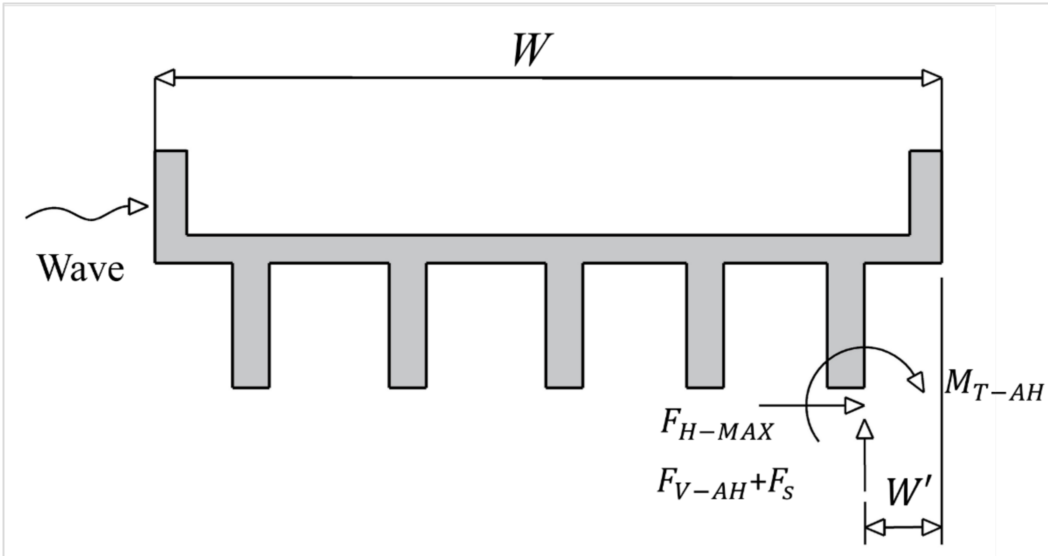

Figure 3. Maximum horizontal force and associated forces, after *(5)*.

The variables shown in Figures 2 and 3 are described as below:

F_{V-max}: Maximum vertical force;
F_{H-max}: Maximum horizontal force;
F_{V-AH}: Vertical forces associated with the maximum horizontal force;
F_{H-AV}: Horizontal forces associated with the maximum vertical force;
F_S: Vertical slamming force;
M_{T-AV}: Moment associated with the maximum vertical force; and
M_{T-AH}: Moment associated with the maximum horizontal force.

3.2. Douglass Equations

Douglass et al. *(13)* proposed the following equations for the horizontal, F_d, and vertical, F_l, hydrodynamic loading on bridge decks. These equations have been used to analyze bridge decks that have been damaged during major hurricane events. For example, Robertson et al. *(14)* used these equations to analyze the damages caused to the bridges in Louisiana, Mississippi and Alabama after Hurricane Katrina. Douglass' equations are the following:

$$F_d = [1 + c_r(N-1)]c_{h-va}\,\gamma\,(\Delta z_h)A_h \qquad [1]$$

$$F_l = c_{v-va}\,\gamma\,(\Delta z_v)A_v \qquad [2]$$

where:
c_r: The reduction coefficient for horizontal load on all bridge girders with a recommended value of 0.4;
N: The number of girders supporting the bridge deck;
c_{h-va}: Empirical coefficient with a recommended value of 1.0;
γ: The unit weight of water;
Δz_h: The difference between the elevation of the crest of the maximum wave and the elevation of the centroid of A_h;
A_h: The area of projection of the bridge deck onto a vertical plane;

$c_{h\text{-}va}$: The empirical coefficient with a recommended value of 1.0;
Δz_h: The difference between the elevation of the crest of the maximum wave and the elevation of the underside of the bridge deck; and
A_v: The area of projection of the bridge deck onto a horizontal plane.

In this study, the forces resulting from these equations are compared to ABAQUS results and the AASHTO equations in order to evaluate the different methods for computing wave forces on bridge decks.

4. METHODOLOGY

In this study, numerical simulations employing the CEL technique were conducted in the commercial software Abaqus in order to reach conclusions that can help mitigate damage in coastal bridges during extreme hurricane events. The accuracy of the numerical results relies on the ability of simulating hurricane-induced waves and bridge conditions accurately. Hence, significant effort was devoted to evaluating the reliability of the model. The work was concentrated on (1) establishing an approach for modeling the desired wave characteristics (i.e., wave height, and frequency) within the CEL simulations, (2) conducting numerical simulations using actual bridge dimensions rather than conducting simulations on scale models as encountered in literature, (3) analyzing a range of foundation flexibilities to determine its effect on the horizontal and vertical forces acting on the superstructure, and (4) comparing results simulations to AASHTO *(5)* equations that estimate wave forces on coastal bridges.

4.1. Numerical Approach

4.1.1. Background Theory

The Lagrange-plus-remap finite element method has been used for modeling fluid dynamic processes *(15, 16)*. The governing equations of fluid dynamics can be written as,

$$\frac{\partial \rho}{\partial t} + \nabla \cdot (\rho v) = 0 \qquad [3]$$

$$\frac{\partial (\rho v)}{\partial t} + \nabla \cdot (\rho v \otimes v) = \nabla \cdot \sigma + \rho b \qquad [4]$$

$$\frac{\partial e}{\partial t} + \nabla \cdot (e v) = \sigma : D \qquad [5]$$

where, ρ is fluid density, v is velocity, σ is the stress tensor, b is the body force, D is the velocity strain and e is the internal energy per unit volume of fluid. These equations can be written in general form as,

$$\frac{\partial \emptyset}{\partial t} + \nabla \cdot \emptyset = S \qquad [6]$$

where, $\emptyset$ is the flux function and S is the source term. Equation (6) has been divided into two equations using operator splitting as,

$$\frac{\partial \emptyset}{\partial t} = S \qquad [7]$$

$$\frac{\partial \emptyset}{\partial t} + \nabla \cdot \emptyset = 0 \qquad [8]$$

which are solved in sequential manner. Equation 7 is analogous to the standard Lagrangian formulation and is called the Lagrangian step. The nodal position changes and the mesh deforms in this step. Equation 8 is the Eulerian step and does not have a time component. In this step, the deformed mesh is moved to the original fixed mesh and then the volume of the material transported between adjacent elements is calculated.

The weak form of these equation has been implemented in ABAQUS and are solved explicitly under the CEL analysis *(17)*. For three-dimensional simulations, the domain is discretized with solid elements, which are usually first order elements with reduced integration in order to expedite the calculations of an inherently costly simulation. Reduced integration can lead to hourglass effects *(16)* that can have detrimental effects on the generated wave and the simulation results. However, hourglass control methods available in ABAQUS can be used to minimize these effects. The pure viscous form of hourglass control is the most computationally efficient form of hourglass control and has been shown to be effective for high-rate dynamic simulations *(17)*.

4.1.2. Wave Generation

Water waves generate due to wind or other types of disturbances in water. Replicating these waves through experimental and numerical means is not a trivial task. Experimentally, waves are generated in a wave tank using two types of wave generators, piston type and flap type. For shallow water waves, the piston-type wave maker is more effective as the piston motion resembles water particle trajectory more closely; while for deep water, the flap type is more effective *(18)*.

Bridges exposed to hurricanes and tsunamis are subjected to shallow water waves. Hence, a numerical approach simulating the piston type wave-maker setup in the laboratory has been considered for this study.

In costal engineering, there are two types of waves, which are: (1) solitary and (2) periodic waves. Solitary waves are waves that propagate without any evolution in shape or size and can be used to represent certain characteristics of storm surge or tsunami generated waves; whereas, periodic waves have been used to represent hurricane induced waves, which are characterized for having shorter wavelengths.

In CEL, the waves' characteristics are defined through the boundary conditions applied at the faces of the domain. Understanding how to adjust the boundary conditions in order to obtain the desired wave characteristics can be a time-consuming learning process for new users. As such, in this report, a detailed procedure to generate periodic waves in the commercial software Abaqus is presented with the aim of facilitating reproducibility of the results and promoting future research work in this topic among the scientific community. The reader is referred to the Abaqus Documentation Manual and literature on the CEL technique to obtain an in-depth understanding of developing models to be used in conjunction with the CEL technique.

In a wave tank, the position of the paddle used to generate waves at a time t is defined as $\xi(t)$. For numerical wave generation, hypothetical paddle conditions are specified at one of the edges of the model. This requires the definition of the velocity, $v(t)$, of the wave paddle trajectory at the hypothetical edge location of the paddle. $v(t)$ is determined by differentiating $\xi(t)$ with respect to t as follows:

$$v(t) = \frac{d\xi(t)}{dt} \qquad [9]$$

A schematic of the wave simulation domain is presented in Figure 4. The initial elevation of the water body is defined as h. The velocity profile is specified along the horizontal direction and it is set constant along the left edge of the domain in order to replicate piston type wave maker conditions. The generated wave has a traveling speed of c which is called the phase velocity.

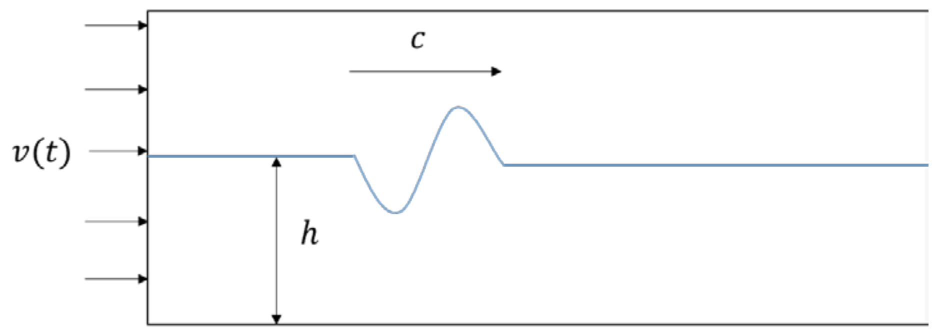

Figure 4. Numerical wave generation schematic.

For modeling the velocity of the paddle trajectory in Abaqus, the velocity direction and magnitude should be provided at the preprocessing stage. In Abaqus CAE, this information can be provided by selecting the edge of interest and defining the direction of the paddle velocity (V1 as indicated in Figure 5). Then, the velocity magnitude can be varied as a function of the simulation time by defining an amplitude function.

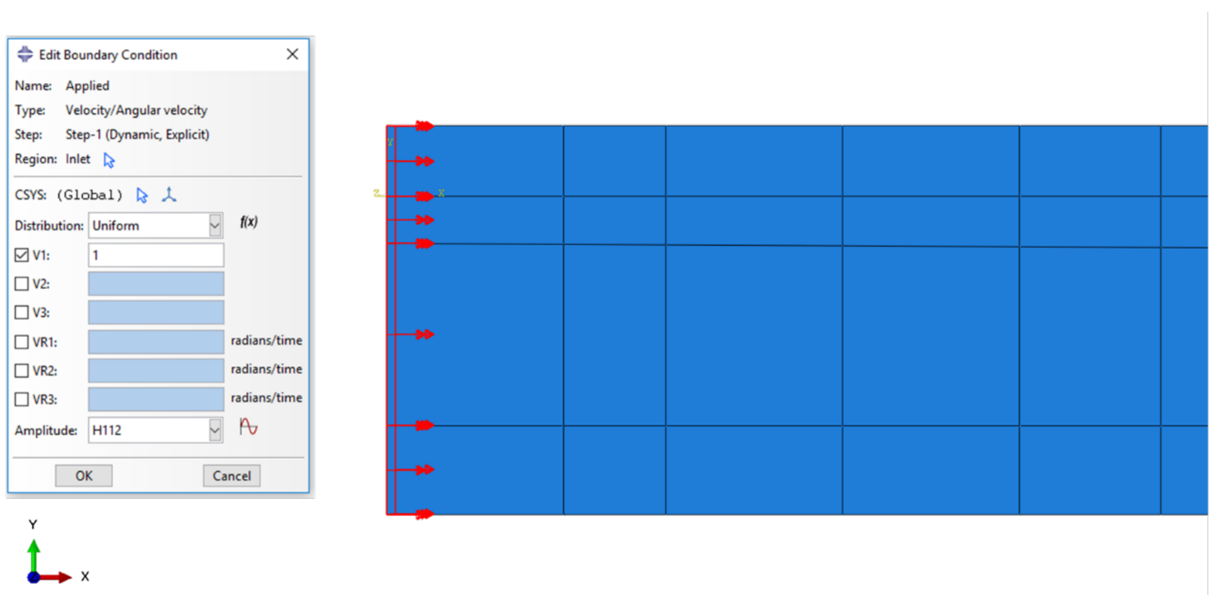

Figure 5. ABAQUS velocity input.

First and second order wave theory: Periodic waves are represented by three variables, which are maximum wave height, H, wave period, T, and initial water depth, h. A schematic of a periodic wave is presented in Figure 6. The wavelength γ can be determined by using these three variables.

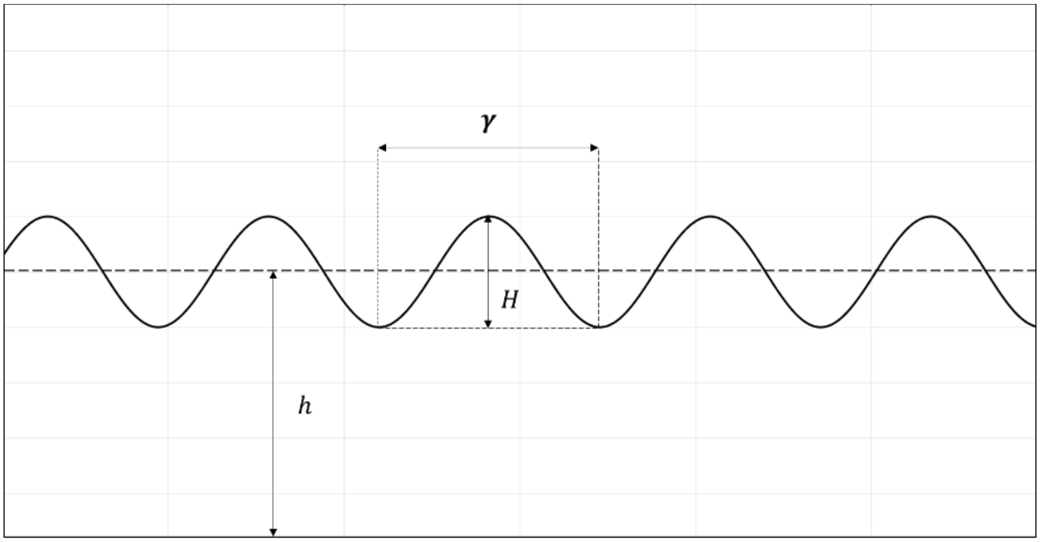

Figure 6. Periodic wave schematic.

For small amplitude waves, the surface elevation, $n(x)$, can be expressed as $n(x) = -\mathrm{asin}(kx - \omega t)$, where $a = \frac{H}{2}$ is the wave amplitude, $\omega = \frac{2\pi}{T}$ is the circular frequency and $k = \frac{2\pi}{\gamma}$ is the wave number. From the linear wavemaker theory *(18)*, the displacement of the wavemaker is determined as:

$$\xi(t) = -\xi_0 \cos(\omega t) \qquad [10]$$

where:

$$\xi_0 = \frac{an_1}{\tanh(kh)} \qquad [11]$$

$$n_1 = \frac{1}{2}(1 + \frac{2kh}{\sin(2kh)}) \qquad [12]$$

The wave number k can be determined from the dispersion relation of Lamb *(19)* as:

$$\omega^2 = gktanh(kh) \qquad [13]$$

Equation 10 represents first order wave theory and only applicable for very small amplitude waves, but not for large amplitude waves. Madsen *(20)* showed that by using this wave maker motion, an unacceptably large free second harmonic will be created that disrupts the desired profile. The free surface elevation will be in form,

Equation 10 has been modified as:

$$\xi(t) = \xi^{(1)}(t) + \xi^{(2)}(t) \qquad [14]$$

The expanded form of the two terms of Equation 14 are:

$$\xi(t) = -\xi_0[\cos(\omega t) + \frac{a}{2hn_1}(\frac{3}{4\sinh^2(kh)} - \frac{n_1}{2})\sin(2\omega t)] \qquad [15]$$

The velocity can be determined as,

$$v(t) = -\omega\xi_0[-\sin(\omega t) + \frac{a}{hn_1}(\frac{3}{4\sinh^2(kh)} - \frac{n_1}{2})\cos(2\omega t)] \qquad [16]$$

The generated waves are Stokes second order waves and theoretically should be in permanent form, i.e., do not disperse over time. Free surface elevation can be written in the form:

$$n(x) = \frac{H}{2}\cos(kx - \omega t) + \frac{\pi H^2}{8L}\frac{\cosh(kh)}{\sinh^3(kh)}(\cosh(2kh) + 2)cos2(kx - \omega t) \qquad [17]$$

This type of wave must satisfy the following criterion to be in permanent form *(18)*:

$$U_r < \frac{8}{3}\pi^2 \qquad [18]$$

where Ursell number is defined as:

$$U_r = \frac{H\gamma^2}{h^3} \qquad [19]$$

These equations are for idealized conditions; however, for numerical simulations with high wave amplitudes, there is a possibility that the generated wave may break and form multiple waves, disrupting its permanent form. This is the case when kinetic energy overcomes the gravity and viscous force. Also, if H is very large with respect to h, the waves tend to break. The basic algorithm to obtain the input velocity profile $v(t)$ can be written as:

1. Assign initial height h, wave height H and wave period T.
2. Determine angular velocity ω, wave amplitude a and ξ_0 from Equations 11 and 12.
3. Determine wave number k from Equation 13 using the Newton Raphson method.
4. Check the Ursell criterion using Equations 18 and 19.
5. Determine velocity $v(t)$ using Equation 16.
6. Determine and check free surface elevation n using Equation 17.

4.1.3. Three-Dimensional Effect

The waves generated in the CEL simulation have shown to be independent of the width dimension (3D effect). This has been demonstrated by generating two waves with different widths and discretization along the third dimension, z-axis. On the first run, a thick width domain was discretized with five elements along the z-direction. On the second run, a thin width domain was discretized with one element. The length dimensions were kept constant in both models. The same velocity profile was applied at the left boundary. The mesh discretization for the thick and thin domains are shown in Figure 7. In Figure 8, the red region represents the initial voids, where the water fraction is zero and the blue region represents the region for which the elements are fully occupied by water. The water fraction changes throughout the simulation; for example, a water amount of 0.5 implies that only half of the volume of an element is occupied by water. The water profile at 4.5 s into the simulation is shown in Figure 9. The water fraction data of the model is processed in MATLAB to determine the wave height profile as a function of time. The maximum wave height throughout the simulation is plotted for both the thick (denoted as 3D) and thin (denoted as 2D) models in Figure 10. It can be observed that the height profiles for both domains are equivalent. For modeling wave-structure interaction, the domains must be larger than the structures width in order to capture the wave impacts on the structure. However, this comparison demonstrates that an in-depth understanding of wave generation can be achieved by considering thin domains, which gives the user the advantage of saving significant computational time.

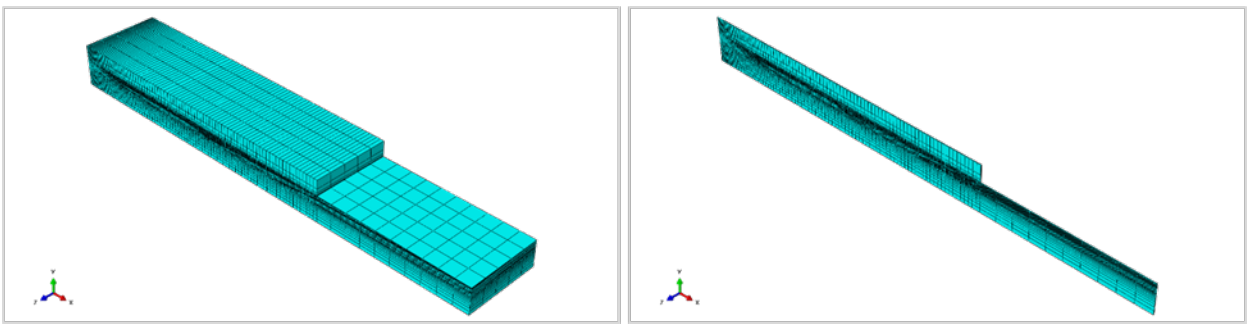

Figure 7. Mesh of a thick and thin domain with equivalent initial conditions.

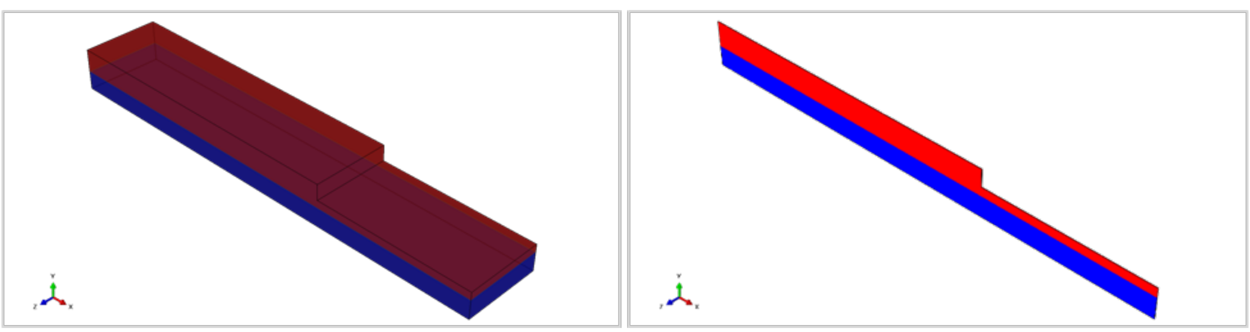

Figure 8. Initial water (indicated in blue) and voids (indicated in red) regions of the simulation.

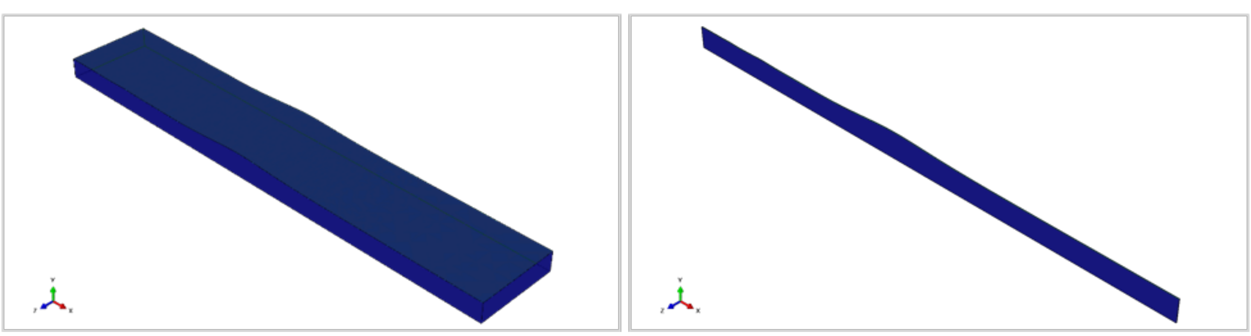

Figure 9. Water condition at t=4.5 s.

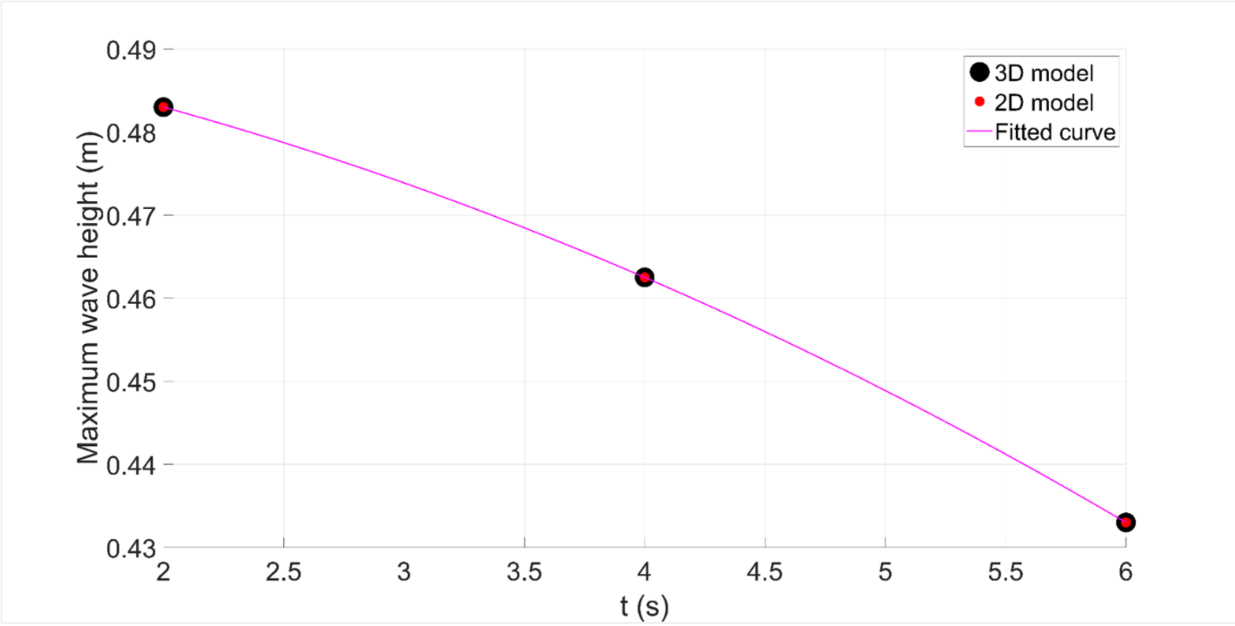

Figure 10. Maximum wave height vs. time.

4.2. Model Development for Wave Generation

The algorithm outlined for velocity generation was coded in MATLAB and evaluated using the following constants presented in Table 1.

Table 1. Input parameters used to generate the velocity wave profile in ABAQUS.

Parameters	Magnitude
Initial water depth, h	$8\ (m)$
Wave height, H	$2.22\ (m)$
Wave period, T	$5.5\ (s)$

Then, the generated velocity profile was applied to the model in ABAQUS to generate the wave numerically. The wave parameters corresponding to these constants are provided presented in Table 2.

Table 2. Wave properties generated using the analytical method.

Parameters	Magnitude
Angular frequency, ω	$1.14239\ (rads^{-1})$
Amplitude, a	$1.11\ (m)$
Wavelength, γ	$40.107\ (m)$
Phase velocity, c	$7.292\ (ms^{-1})$
Ursell number	6.97

The velocity profile from Equation 16 is plotted in Figure 11 and the theoretical free surface elevation (Equation 17) at time $t = 30$ s is illustrated in Figure 12. The profile of free surface elevation indicates that although a primary wave, i.e. a wave having only one amplitude and wavelength, and a secondary wave have been generated by the algorithm, the secondary wave has negligible effect. This result creates confidence that generated waves within the CEL simulation will not likely break and/or create waves with different characteristics.

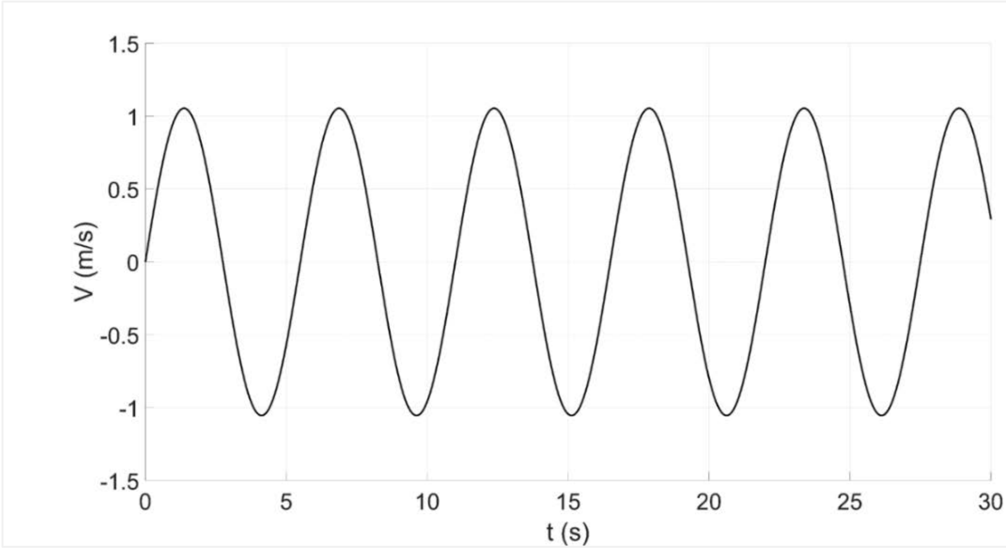

Figure 11. Velocity profile at boundary condition.

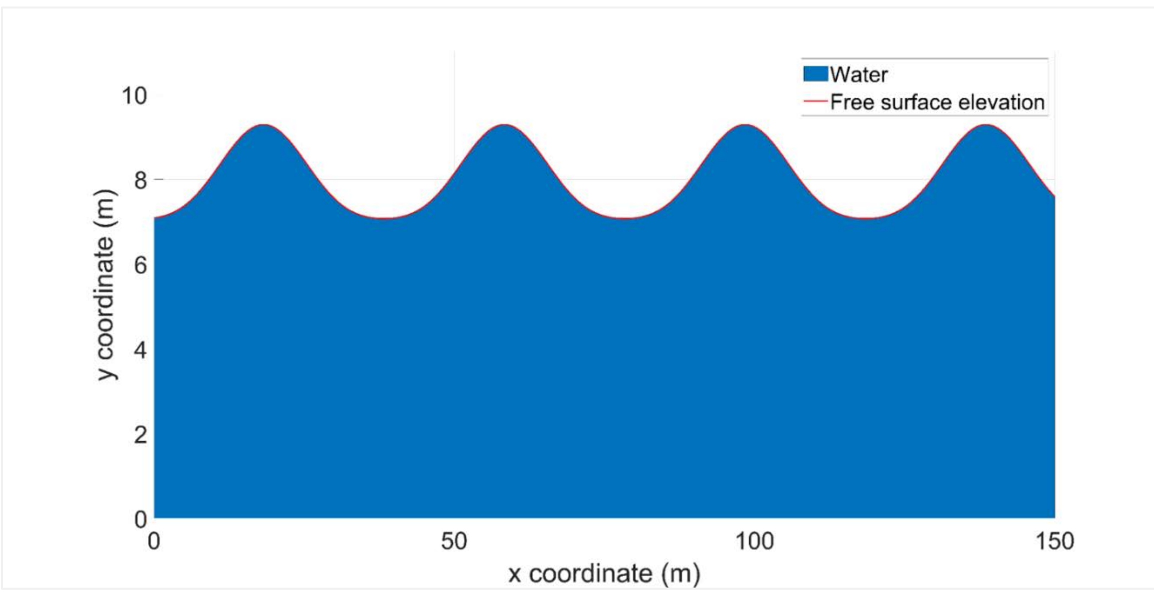

Figure 12. Free surface elevation at time 30 s.

A 200 m long domain was created in Abaqus to test the wave generation approach. The model was partitioned into several domains as illustrated in Figure 13. The domain details have been presented in Table 3. The boundary condition and loading applied to this domain is presented in Figure 14. The velocity v_x is applied at the left end, acting as an inlet to generate the wave.

Table 3. Domains defined in the ABAQUS model.

Variable	Domain Details	Magnitude
h	Represents initial water depth from the bottom surface. It is essentially equal to the h value used in Table 1.	0.32 (m)
N_{sb}	A lower horizontal partition to consider "no slip boundary condition". Requires fine mesh as there will be velocity gradient as a result of boundary layer.	1.5 (m)
a_{cc}	The free surface profile will be generated within the range $(h-a) \leq n \leq (h+a)$ analytically. For numerical wave generation this has been considered as, $(h-a_{cc}) \leq n \leq (h+a_{cc})$ where $a_{cc} > a$. This section will be subjected to high velocity gradient; hence, a fine mesh is required.	1.5 (m)
W_{mr}	Consideration for wavemaker. Only the velocity along the y axis = 0 for the bottom surface of this region. As this region is very close to inlet, a fine mesh is required.	5 (m)

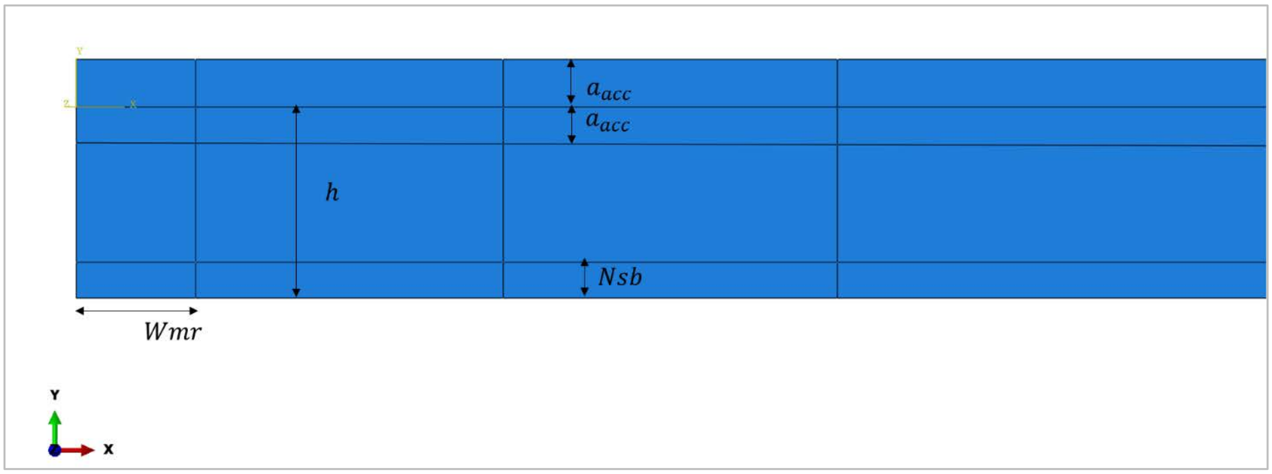

Figure 13. Model Partition (Zoom at the 50 m portion from right edge).

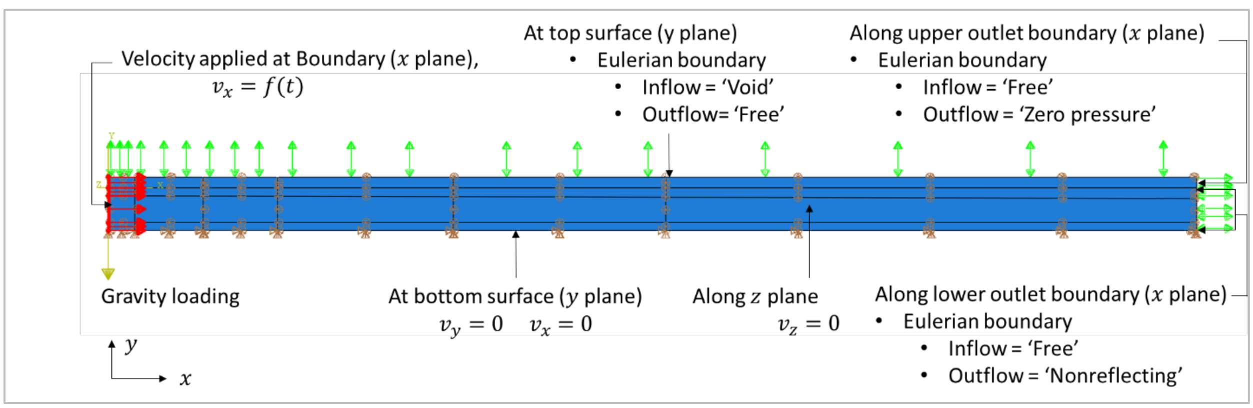

Figure 14. Boundary conditions.

It must be noted that the wave profile is expected to be disrupted at the right end (outlet), implying that the wave characteristics vary as the wave travels from the inlet to the outlet. This disruption has been observed in two forms: (1) lost wave shape and (2) wave reflection.

Numerical tests have revealed that the wave reflection near the outlet can completely disrupt the desired wave shape. This condition amplifies when the velocity along the x-axis at the outlet is set to zero. This problem can be mitigated by imposing Eulerian boundary condition, "Non-reflecting" outflow *(17)*, at the lower portion of the outlet (from the bottom surface to the initial water depth level, h). For the upper section (from h to the top edge), the "zero pressure" outflow has been considered which essentially allows the water above h to flow out of boundary without reflecting at all. These boundary conditions have some impact on the wave shape but minimize wave reflection. Thus, for modeling wave-structure interaction, the exhibited disturbance condition requires that the structure be placed away from the outlet to guarantee that the desired wave impacts the bridge.

The recommended mesh discretization is illustrated in Figure 15, depicting the initial water elevation and voids. The mesh was finer within the first 5 m the right of the left edge (5 m in a 200 m length, 2.5% of the total length) as the waves form within this region. The mesh was then coarsened along the length. The 3-dimensional representation of the model is presented in Figure 16, only one element was used along the z-axis in order to save computational effort.

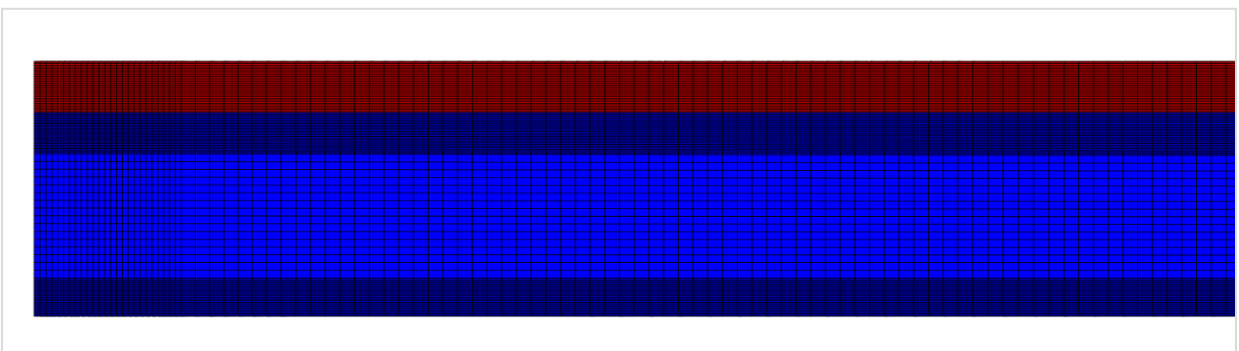

Figure 15. Meshing with initial water (zoomed at the 50 m portion from the right edge).

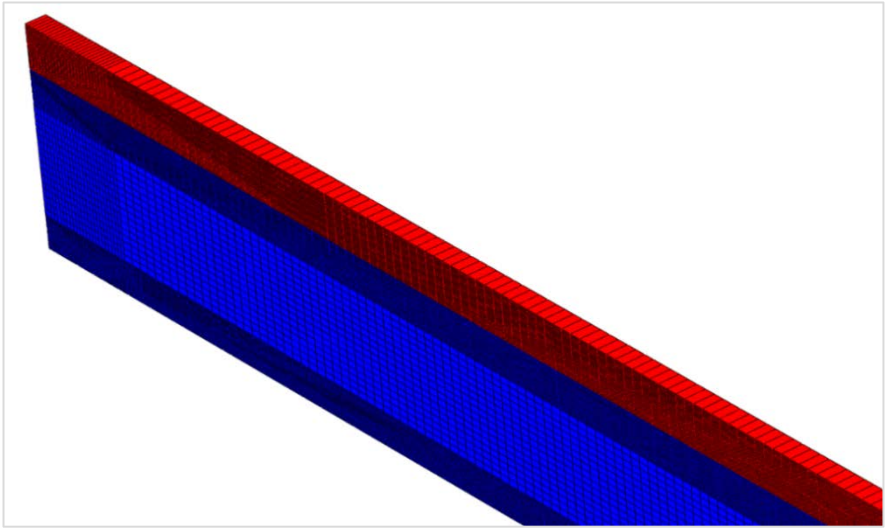

Figure 16. 3D simulation domain.

The waves generated are illustrated in Figure 17 from 3 s to 15 s and in Figure 18 from 18 s to 30 s. These figures help to illustrate the lifecycle of a wave, which can be subdivided into 3 stages: (1) wave generation, (2) wave stabilization, and (3) wave dissipation.

The first generated wave had a very low amplitude and dissipated after forming as shown in Figure 17. This phenomenon of lower amplitude for the first generated wave has been also observed experimentally *(15)*. The first wave eventually dissipated as shown at t=15 s. The 2nd wave presumably dissipated due to its interaction with the first wave at the right boundary as shown in Figure 18. The subsequent waves appeared to be more stable than the initial waves.

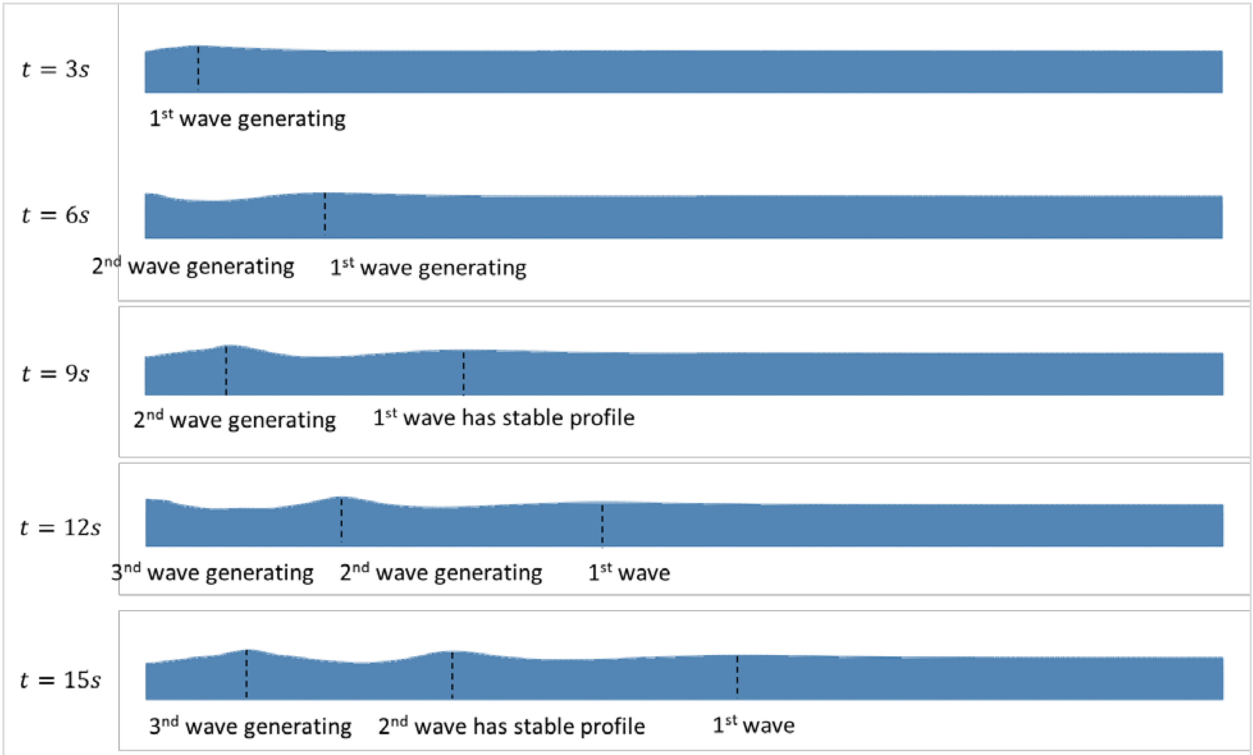

Figure 17. Wave profile for t=3 s to t=15 s.

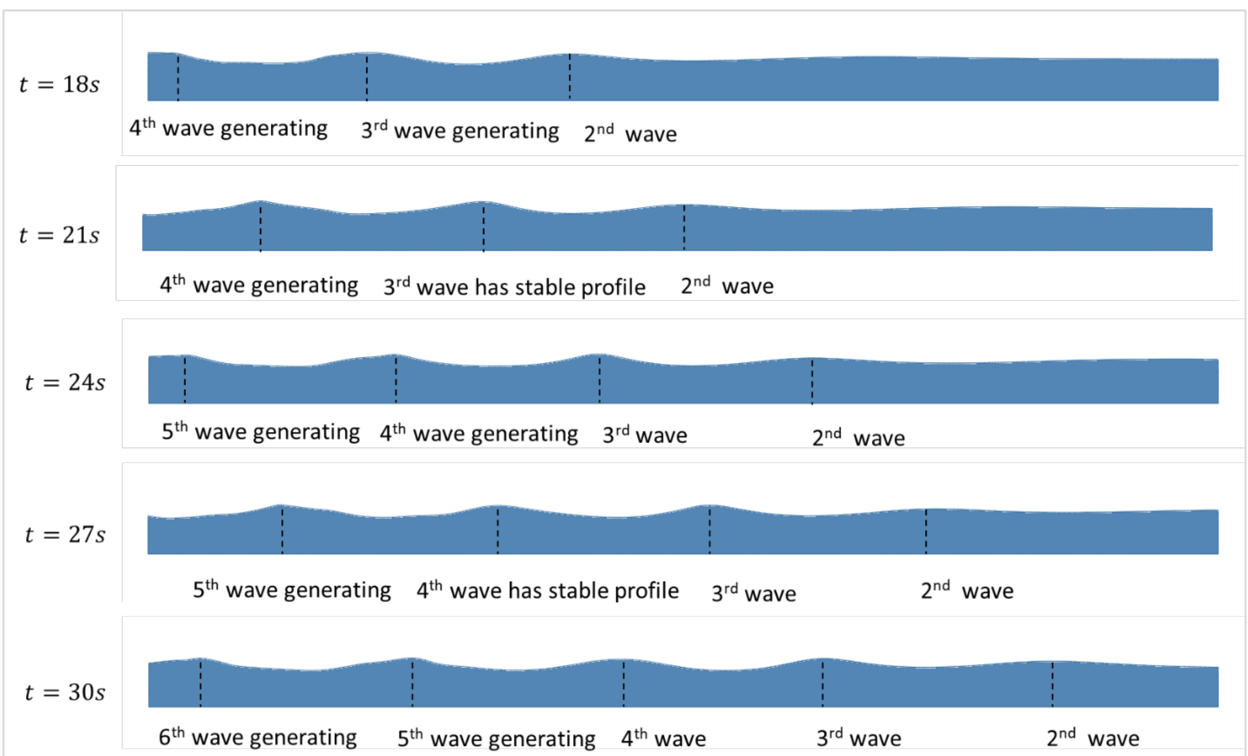

Figure 18. Wave profile for t=18 s to t=30 s.

As it was mentioned above, at the right most boundary, a non-reflecting boundary condition was used, which prevented the waves from reflecting. However, this boundary condition did not replicate ideal non-reflecting conditions and impacted the behavior of the traveling waves. The velocity magnitude at time $t = 30\ s$ (see Figure 19) can be used to understand the interaction between the right boundary and the 1st wave. The velocity profile of the right most wave, which is the 1st wave, seems to be disturbed as compared to the velocity profile of the rest of the waves. This disturbance has some effect on all incoming waves. For a wave-structure interaction, this situation can be omitted if a domain of considerable length is chosen; however, at the expense of a higher computational cost.

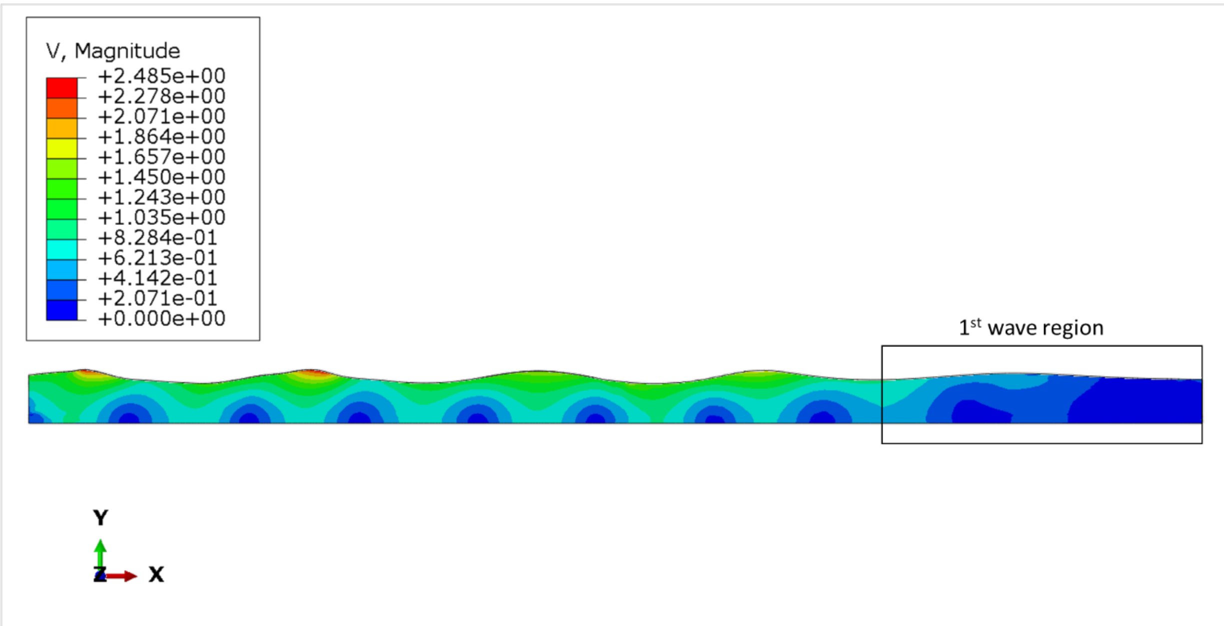

Figure 19. Velocity magnitude profile at time=30 s.

The shape of the waves, i.e. free surface elevation, has been illustrated in Figure 20, as a function of time and length. The left end of the domain (x=0 m, where the boundary conditions are applied) shows a sinusoidal free surface elevation, characteristic of a permanent form; however, this form is lost throughout the length of the domain. The wave amplitude decays along the length of the domain as shown in Figure 20.

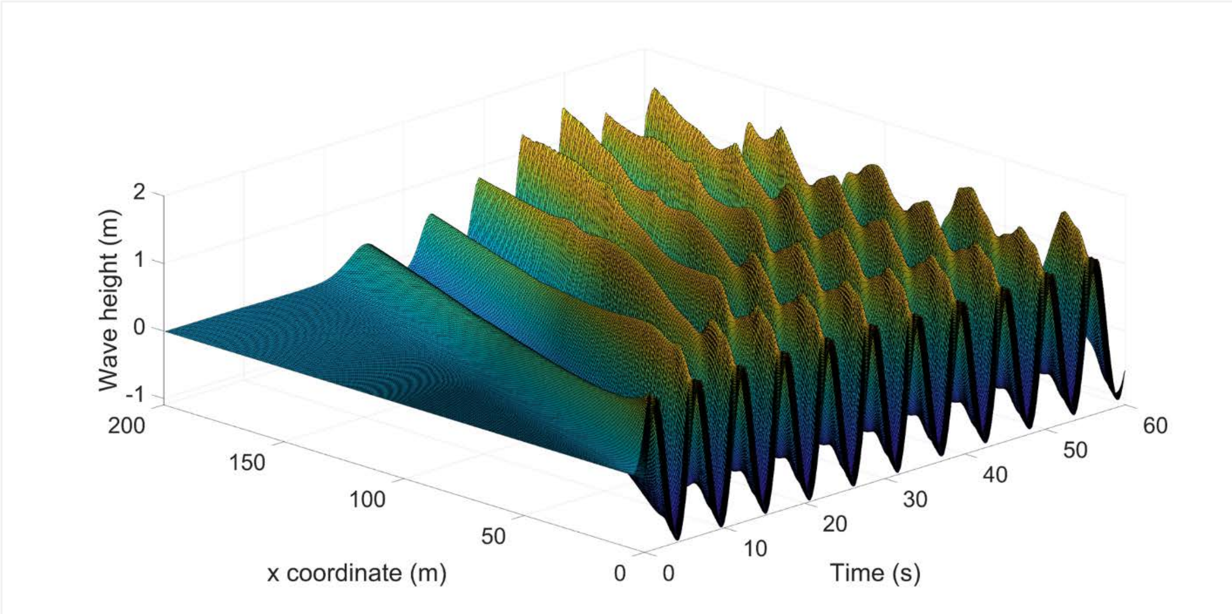

Figure 20. Free surface elevation vs. time vs. space.

As the wave profile is strongly dependent on location, the bridges or structure that will be impacted by the waves must be placed at a location in which the simulated waves have not lost the desired amplitude. For example, for a 200 m length domain, a good location for the bridge would be 39 m (about 20% of the total length). Figure 21 plots the free surface profile at this location (x=39 m) as function of time, illustrating that the waves, after the third wave, remain stable throughout the length of the simulation.

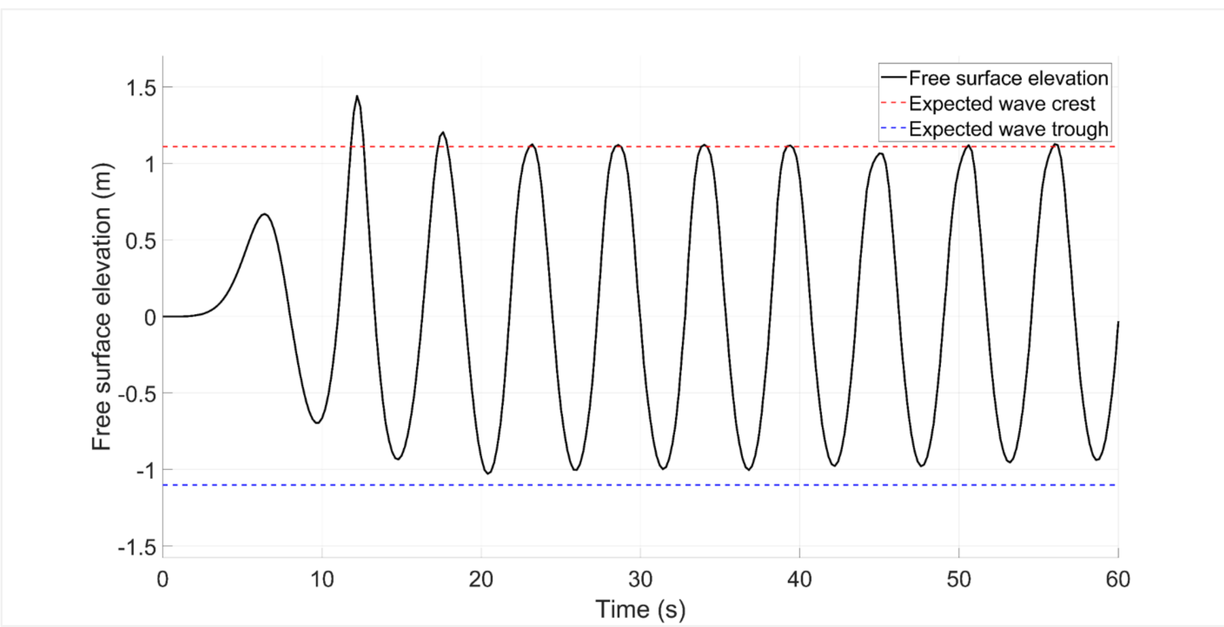

Figure 21. Free surface profile at x=39 m.

A study on mesh sensitivity was conducted for the generated wave for 2 different mesh sizes in which the length of the coarser elements was varied from $1m$ to $2m$. Figure 22 shows that the results do not seem to deviate significantly but overlap at various points of the plot.

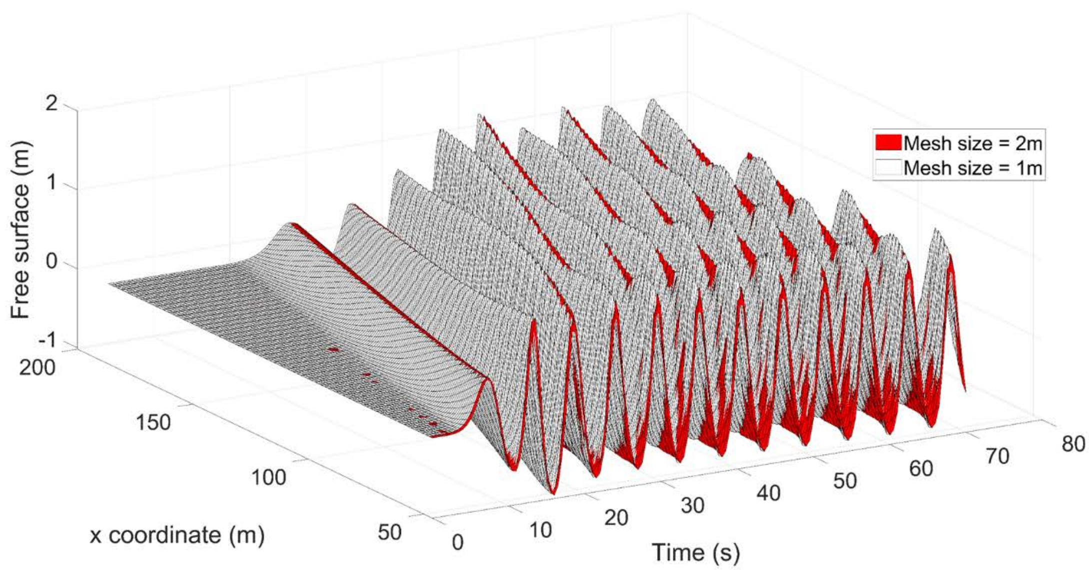

Figure 22. Mesh sensitivity analysis.

4.3. Bridge Models

The analysis revolved around two major highway bridges along the U.S Gulf Coast that were severely damaged during hurricane Katrina in 2005, (a) the U.S 90 highway bridge over Biloxi-Bay and (b) the US. 90 St. Louis-Bay Bridge. The span dimensions are illustrated in Figures 23-24. Unlike other simulations available in literature, the models were based on the actual dimensions of the bridge (see the Appendix for detailed drawings of St. Louis Bridge). The main difference between these two models is the shape of the superstructure. Supports were modeled as rigid at the offshore corners and as simple supports at the onshore corners to agree with the analyses available in literature.

The I-10 bridge across Biloxi-Bay was a simply supported span bridge with 15.9 m long spans across most of its length. The bridge had two 8.7 m wide spans placed side by side with a distance of 0.1 m. It is likely that each span behaved separately since there was no connection between them. The Biloxi-Bay Bridge has a total of 10 I-type girders. This analysis modeled a typical span of the I-10 Bridge across Biloxi-Bay is shown in Figure 23. The total height of the deck was 1.1 m and the bottom of the girders had a width of 0.51 m. The deck thickness was defined as 0.34 m.

The U.S 90 bridge across St. Louis Bay was also modeled as a simply supported span bridge with a 15.9 m long span, as shown in Figure 24. The bridge had two 8.7 m wide spans placed side by side with 0.1 m. The U.S 90 bridge across St. Louis Bay has a total of 8 T-type girders. The total height of the deck was 1.1 m and the bottom of the girders had a width of 0.48 m. The deck thickness was also defined as 0.34 m. The dimensions and configurations of these two bridges are provided in Table 4.

The wave characteristics of the model were defined according to those reported by Chen et al. *(21)*. They estimated that for extreme catastrophic events, such as Hurricane Katrina, the relatively small maximum wave height and peak period at the U.S 90 Bridge over Biloxi-Bay, can be assumed of 2.6 m and 5.5 s, respectively.

Table 4. Dimensions and configurations of the I-10 and U.S 90 bridges.

Bridge	Span Length (m)	Span Width (m)	Deck Thickness (m)	Girder Type	Girder Height (m)	Girder Width (m)
I-10	15.9	8.7	1.1	AASHTO Type III	0.75	0.5
U.S 90	15.9	8.7	1.1	Slab	-	-

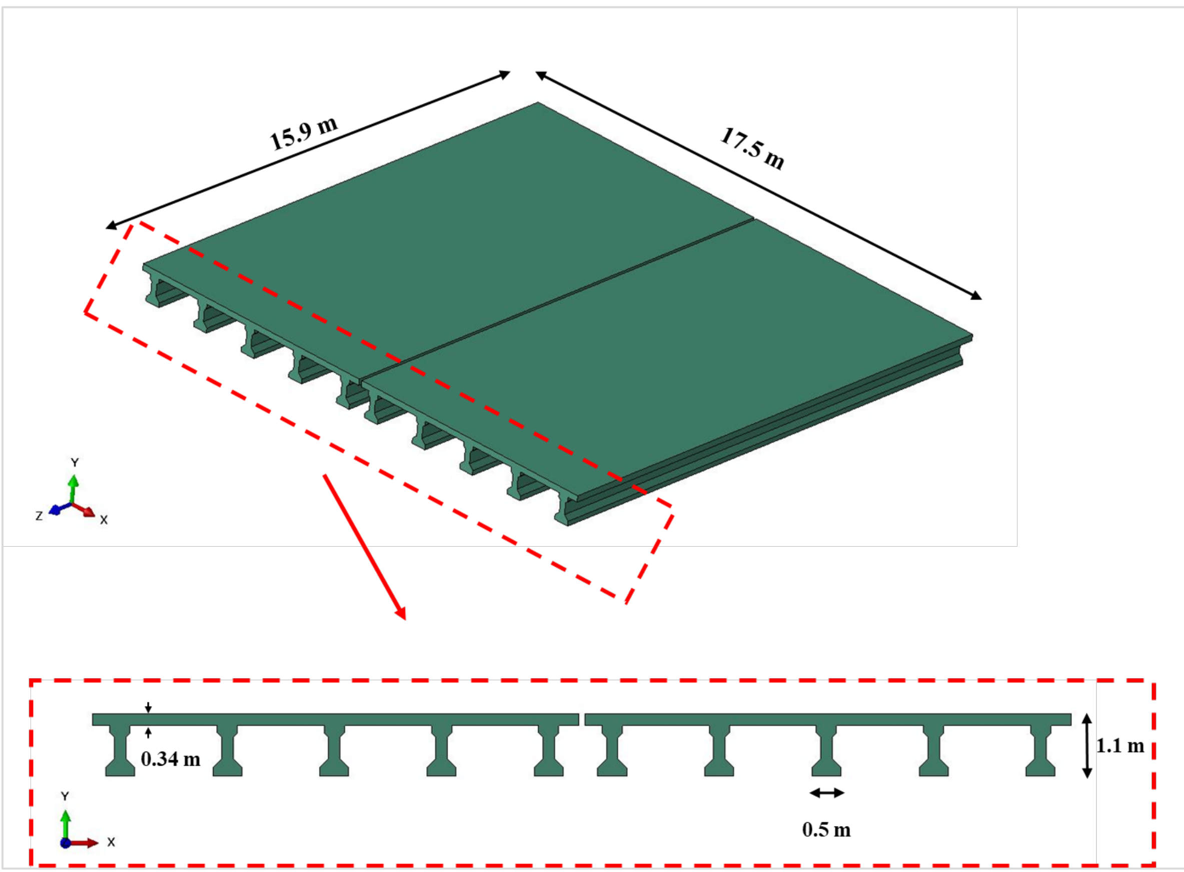

Figure 23. Deck Configuration for the I-10 Biloxi-Bay Bridge.

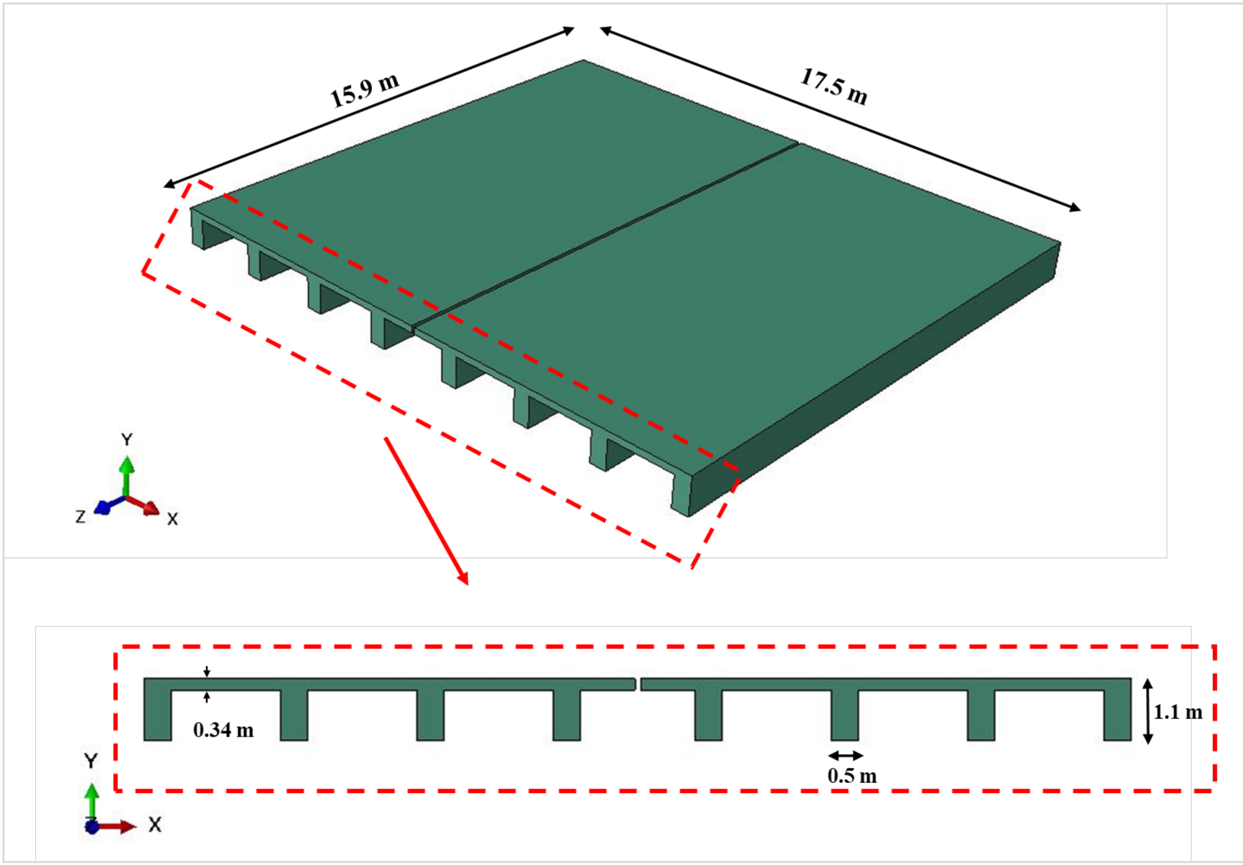

Figure 24. Deck Configuration for the US-90 St. Louis-Bay Bridge.

Figure 25 shows the domains of the Coupled Eulerian-Lagrangian (CEL) analysis that were defined at the beginning of the analysis. Solid brick elements were used to model the bridge components and tie constraints were used to model the interaction between the surfaces of the superstructure and substructure.

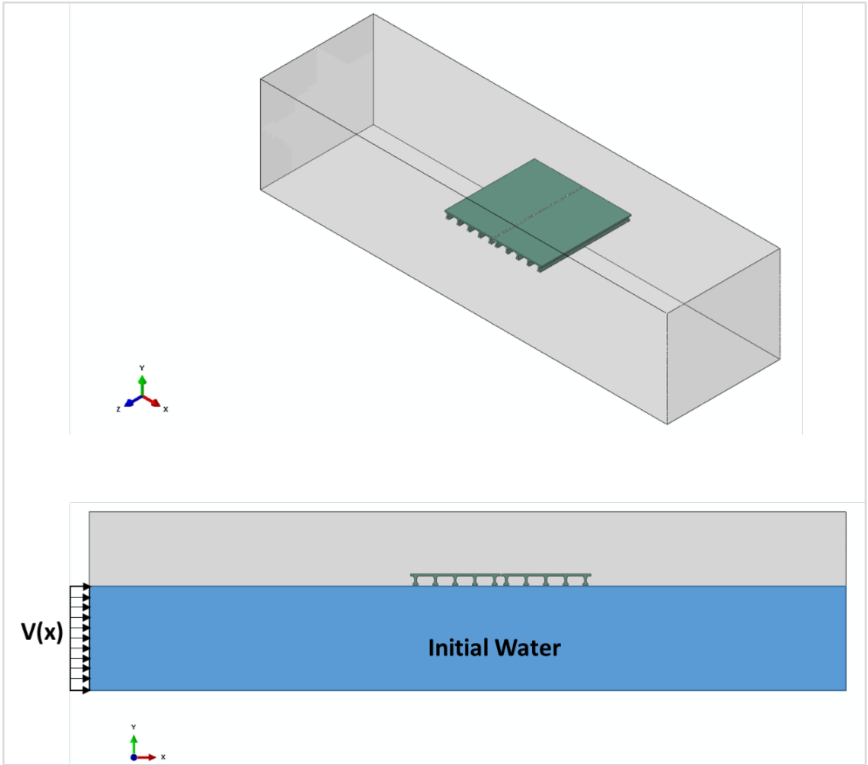

Figure 25. CEL simulations domain: Green domain is Lagrangian, Blue (water) and Gray (initial voids) are Eulerian.

4.4. Parametric Study

4.4.1. Flexibility of the Substructure

The flexibility of the foundation is expected to have a significant effect on the horizontal and vertical forces acting on the superstructure condition. The rigid conditions that have been assumed in previous studies are believed to overestimate the force demands on the bridge superstructure. As such, foundation variations were conducted on the Biloxi-Bay Bridge model described in the former section. The substructure was introduced to the model by defining pier caps and piers with the dimensions specified in Figures 26.

Three pier lengths were considered for each model, 7.6 m, 10.6 m and 13.6 m, as shown in Figure 27. The water level elevation was defined at the bottom of the superstructure as post-Katrina investigations revealed that this was a common characteristic for bridges that were severely damaged during the hurricane.

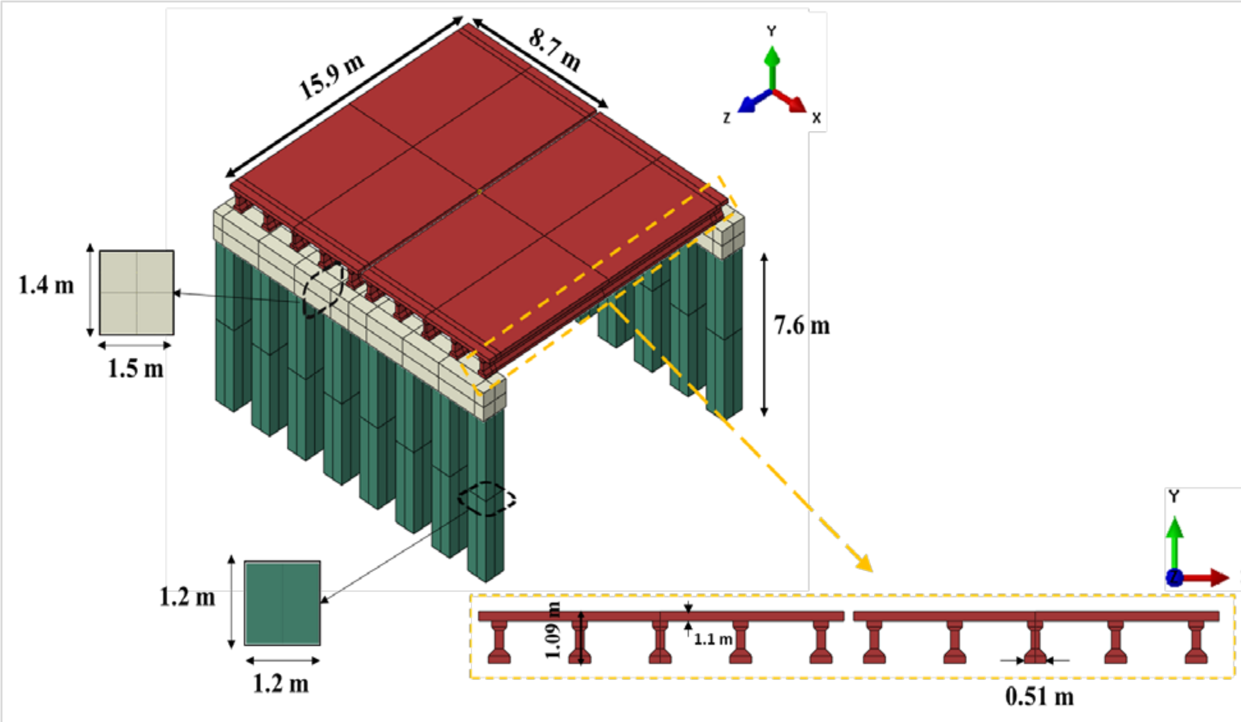

Figure 26. Biloxi-Bay Bridge model with flexible substructure conditions.

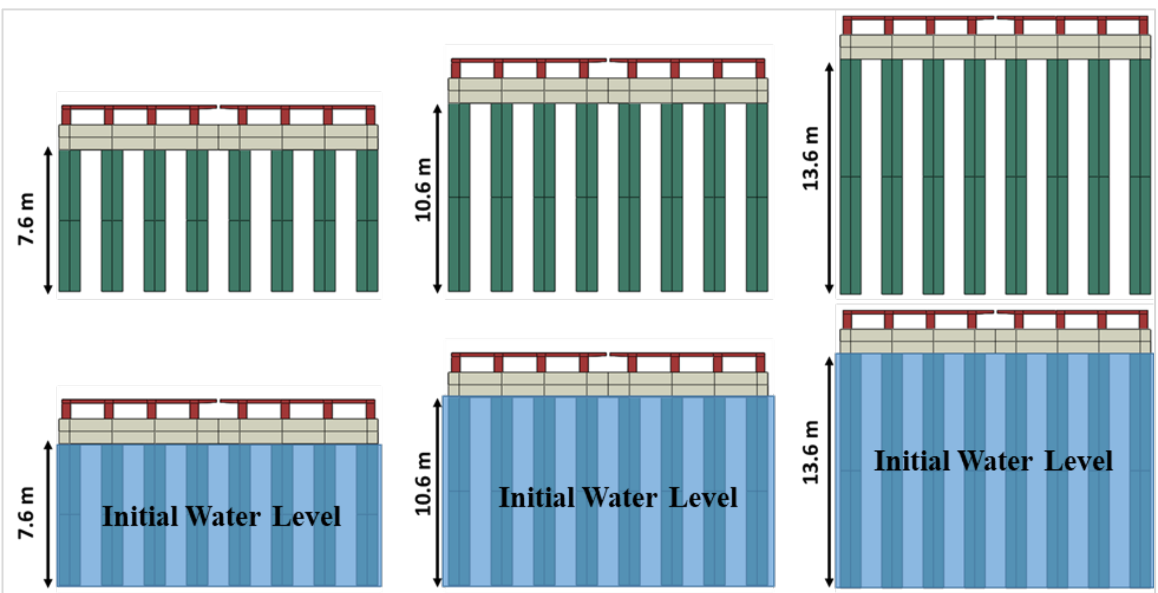

Figure 27. Pier length dimensions and water elevation for the models with flexible substructure conditions.

4.4.2. Variation in the Boundary Conditions

Variations in the model's geometry and boundary conditions were proposed in order to properly quantify the force demands at the pier caps, which are the structural members that tend to fail during extreme hurricanes. A typical pier cap on a multi-span bridge holds the load of two spans, but formers models only apply the load coming from one span. The I-10 Bridge across Biloxi-Bay model with 10.6 m piers was modified as shown in Figure 28 in order to account for the load coming from both spans. The bridge model had two 10.4 m wide spans (half of actual span dimensions) supported by the pile caps. Symmetric boundary conditions were applied at the ends of the right and left span (mid span in the actual bridge) in order to reduce the computational time associated with the model. The model is impacted by waves traveling perpendicular to the length of the model as illustrated in Figure 29.

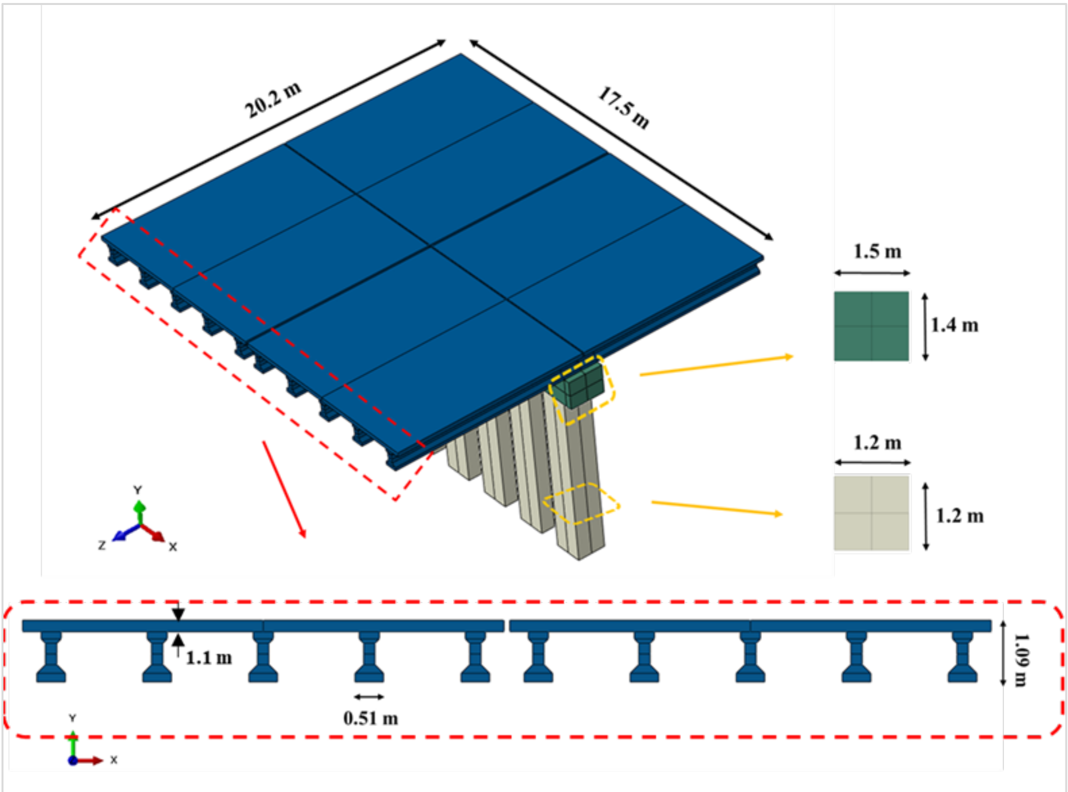

Figure 28. Configuration of the Biloxi-Bay Bridge.

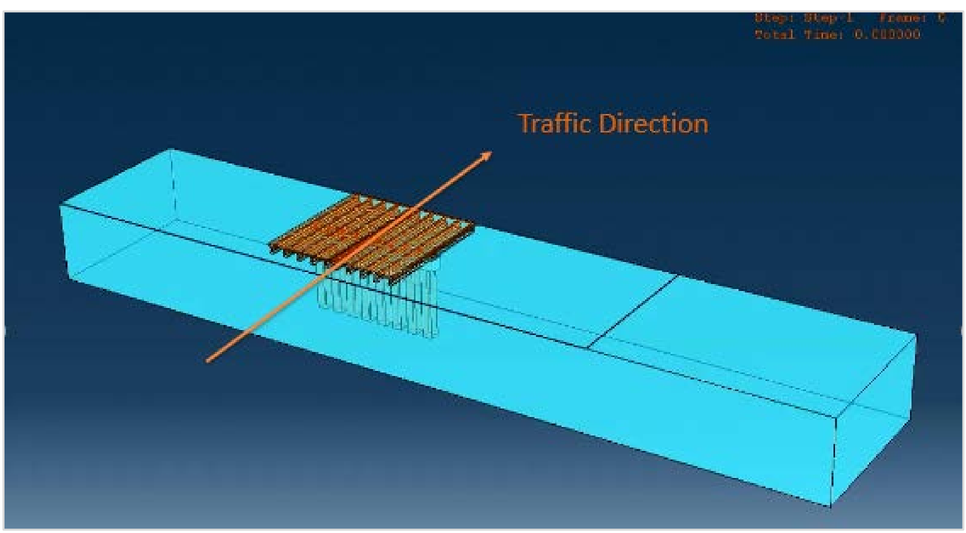

Figure 29. Biloxi-Bay bridge model within the fluid domain.

5. ANALYSIS AND FINDINGS

5.1. Rigid Support System

Figure 30 shows a sequence of images illustrating the impact of the wave on the bridge structures at four discrete times. The wave traveled transversal to the bridge deck and made impact with the front face of the deck at time t_1. Then, the wave crossed over the bridge from time t_2 to time t_6. The contour plots in Figure 30 show the displacement magnitude of the bridges. Although the wave behaves similarly in the simulations of the St. Louis and Biloxi bridges, the displacement history of the deck is different. The Biloxi-Bay bridge deformed more at the initial time of impact, at time t_1; while at time t_4, after the wave crossed over the decks, the deformation on the second span of the St. Louis Bridge was larger.

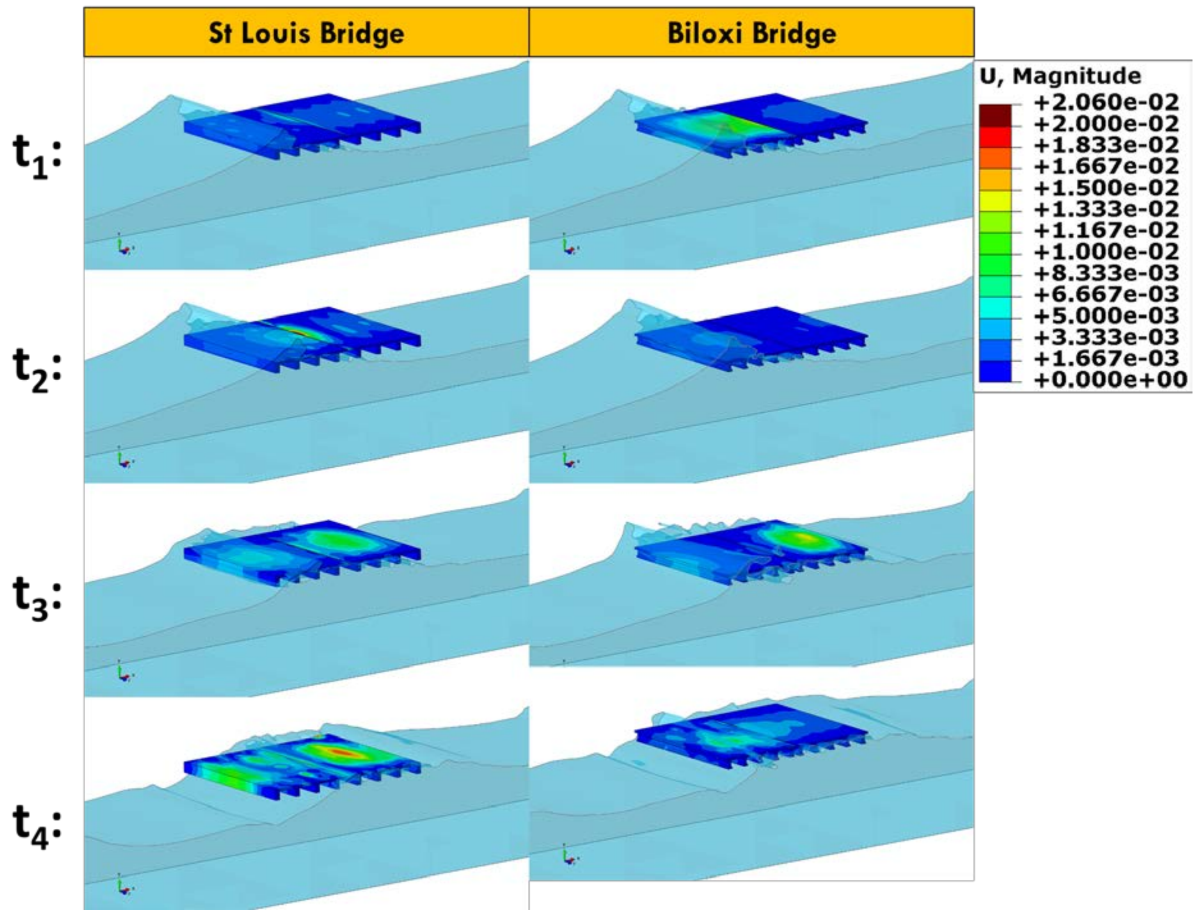

Figure 30. Wave impact sequence on St. Louis and Biloxi-Bay bridge with rigid supports.

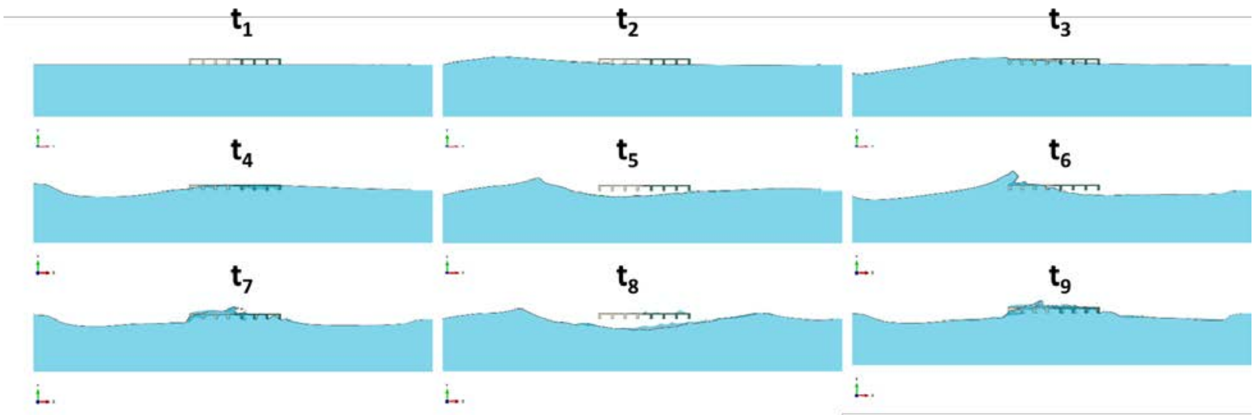

Figure 31. Elevation view of wave impact sequence on St. Louis and Biloxi-Bay bridge with rigid supports.

Figure 31 provides the history of the wave from the left edge to right edge of the domain. The image shows that that the bottom of the superstructure coincided with the initial water level at the beginning of the simulation. As the first wave (previously described as a rapidly dissipating wave or weak wave) was generated, the water level raised and submerged the superstructure between discrete times t_3 and t_4. Then, the second wave was generated at t_4, which approached the structure at t_5, and impacted the front deck at t_6. The cycle was repeated again from t_7 to t_9.

The stresses at the interface between the superstructure and substructure were integrated over the interface area in order to determine the history profile of the uplift and shear forces acting on the superstructure. The magnitude of the reaction forces normalized with respect to bridge weight are presented in Figures 32-33. Figure 32 provides the results for the front decks, while Figure 33 provides the results for the rear decks. It can be observed that the differences in the uplift forces between the front decks of both bridges were negligible; however, significant discrepancies were observed in the uplift forces of the rear deck. The peak magnitude of the Biloxi-Bay bridge in the rear deck was about twice the peak magnitude of the St. Louis Bridge. Nevertheless, the front decks, which experienced a direct wave impact, showed a larger maximum uplift force than the rear decks.

The magnitude of the forces was significantly higher than the bridge weight, which is in agreement with the damage experienced by these bridges during Hurricane Katrina. However, as the FE model supports were rigid, the force magnitudes were presumably overestimated. The maximum uplift force was 12 times the weight of the bridge, which suggests that the weight of the superstructure would not be sufficient to hold the superstructure in place if roller supports had been defined.

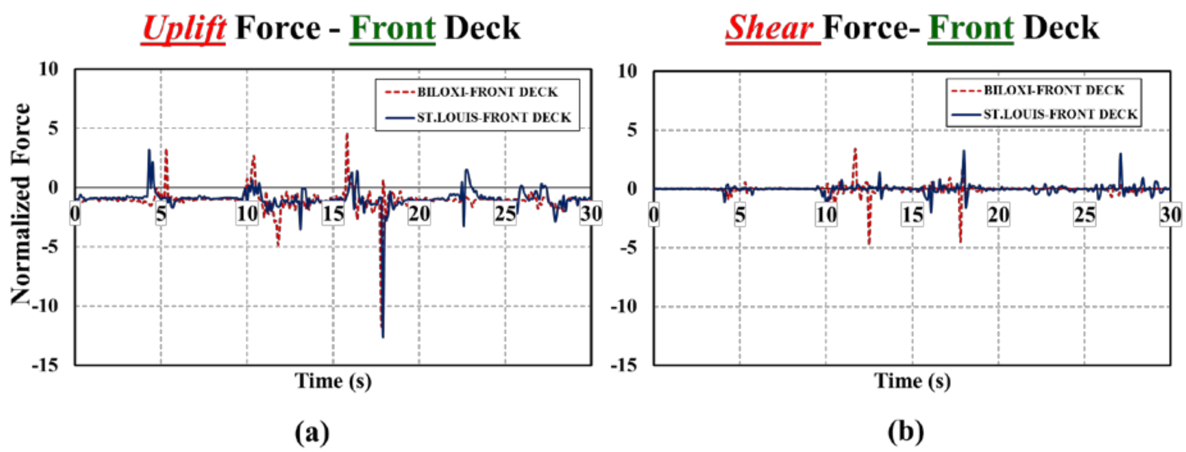

Figure 32. Normalized Uplift and shear force on front deck.

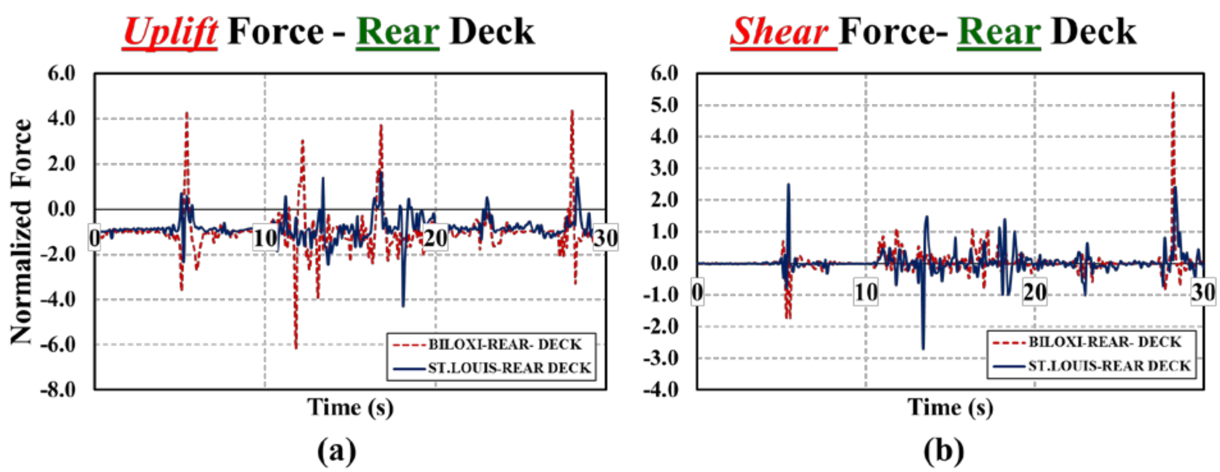

Figure 33. Normalized Uplift and shear force on rear deck.

5.2. Flexible Support System

A snapshot of the simulation history for the models with different pier heights is illustrated in Figure 34. Although all the models had different water elevations, the wave amplitude that impacted the superstructure was kept the same. Figures 35 and 36 show the uplift and shear force demands in the three models. It can be observed that the force demands were not proportional to the length of the piers, as the model with the 10.62 m height piers shows the largest amplitudes for both uplift and shear forces. The peak demands were confirmed to occur at instances in which the waves made direct impact with the superstructure. The largest spike in the uplift force occurred at 8 s (see Figure 35), after the first wave impacted the bridge. However, the magnitude was about 4 times than the rest of the spikes. Further investigation should be conducted to determine if this behavior was a numerical artifact.

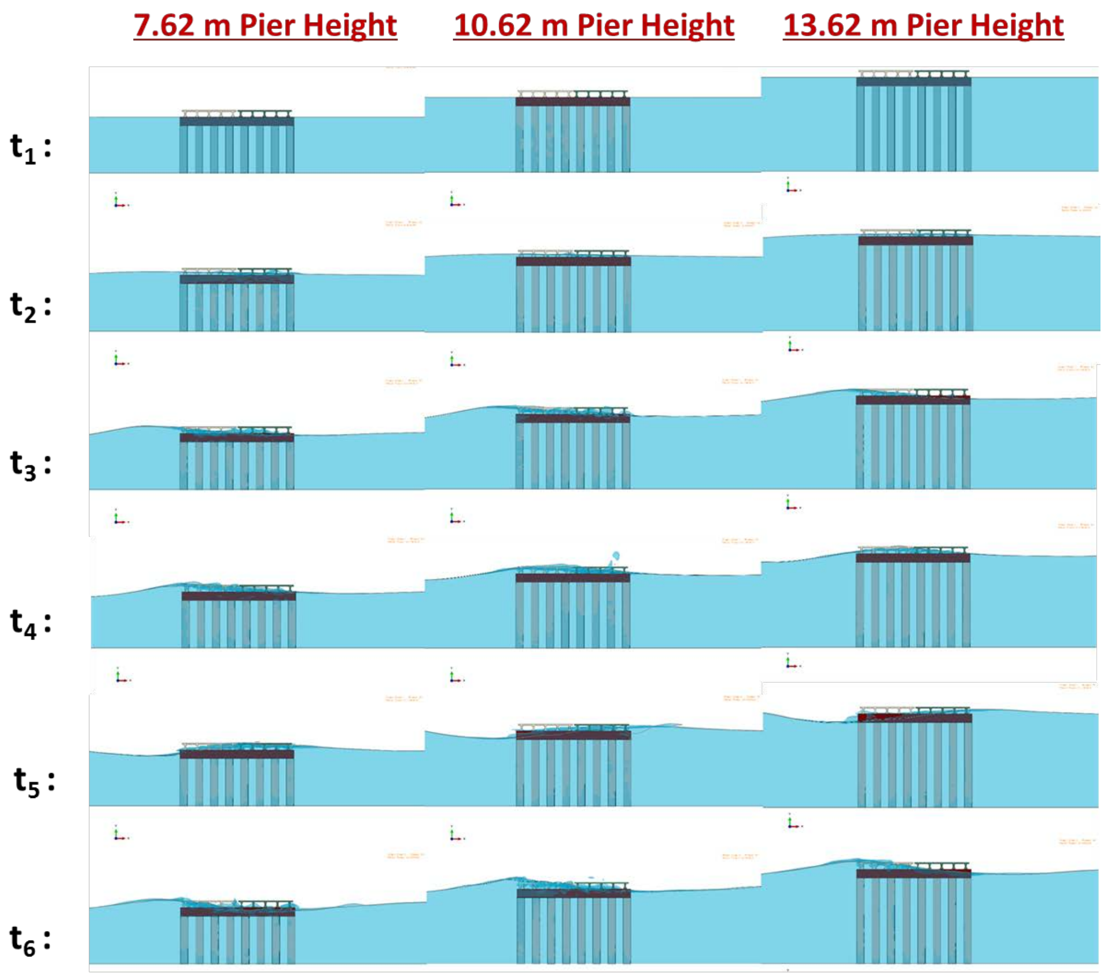

Figure 34. Normalized uplift and shear force on rear deck.

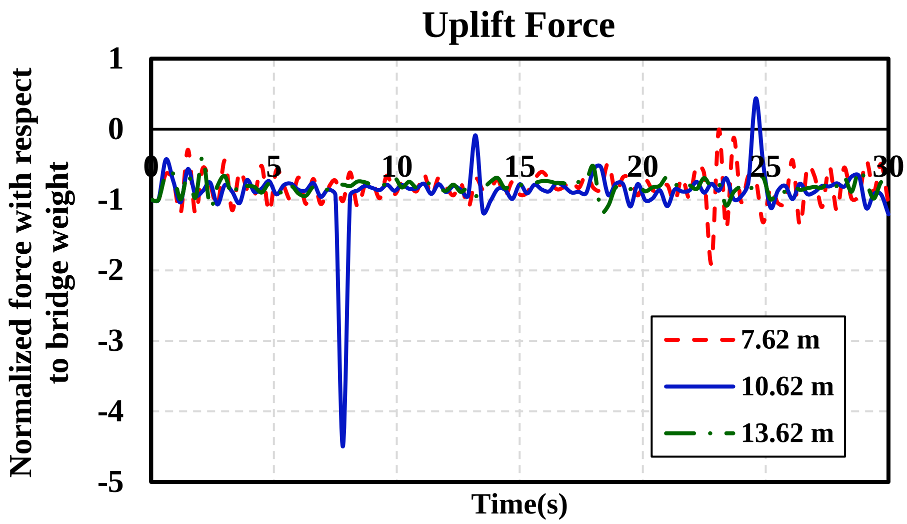

Figure 35**. Uplift forces for different height of piers.**

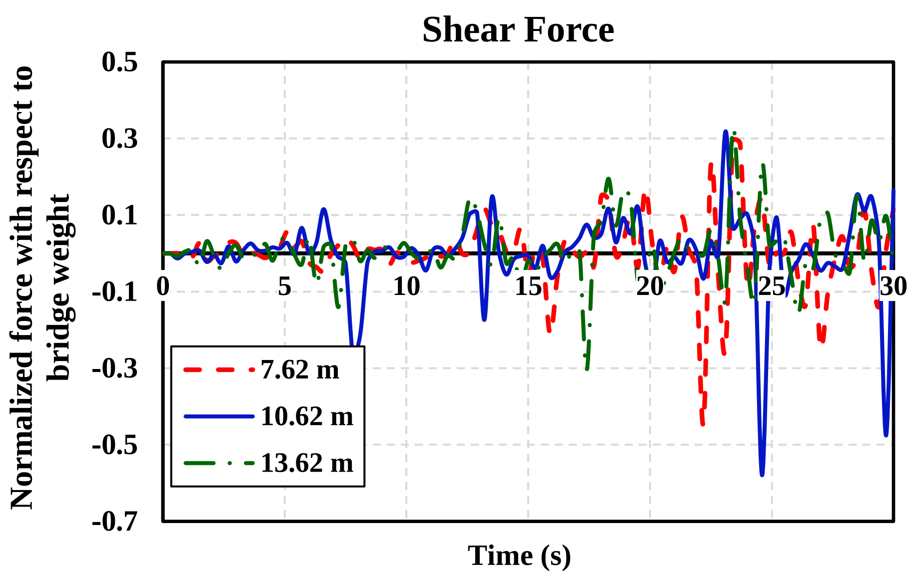

Figure 36. Shear forces for different height of piers.

5.3. One Pier Model

The results for the one pier model were compared against the AASHTO and Douglas equations described in the Introduction. Figures 37 and 38 plot the normalized uplift and shear forces on the front deck, while Figures 39 and 40 plot these forces on the rear deck. The front deck showed larger demands, which agrees with the previous simulations conducted in this study. Overall, the results of the simulation were bounded by the AASHTO and Douglas equations. However, spikes that exceeded the estimates provided by these analytical equations were observed occasionally throughout the history of the simulations. These spikes are large in magnitude and tend to be 3-5 larger than the weight of the bridge. Like the previous results, these spikes coincided with instances of wave impacts. Further numerical analyses, flume tests, and field measurements are required to determine the cause of these spikes.

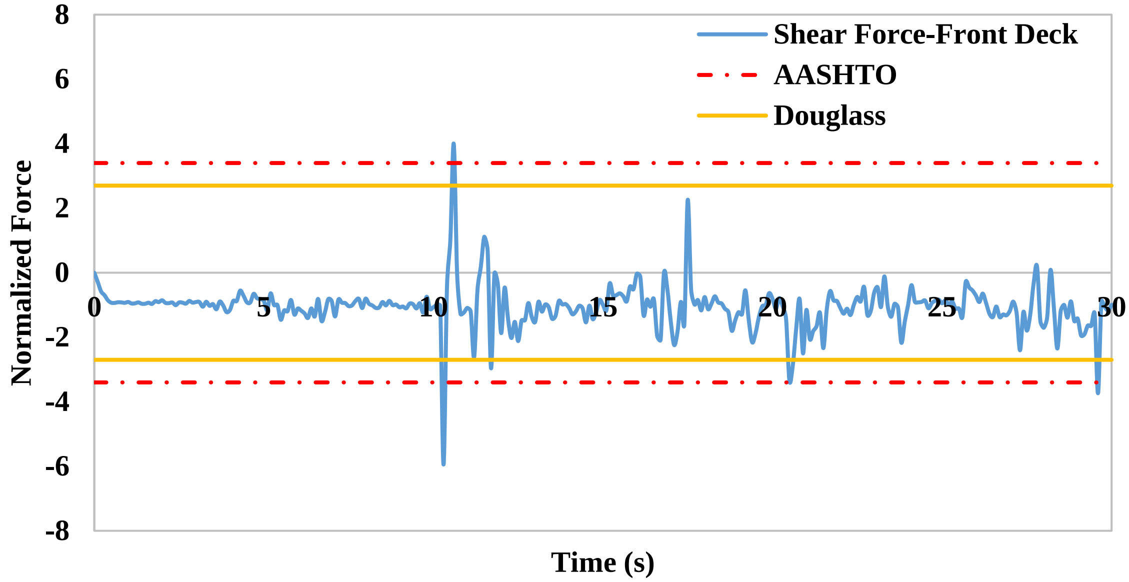

Figure 37. Uplift Force-Front deck of one pier model.

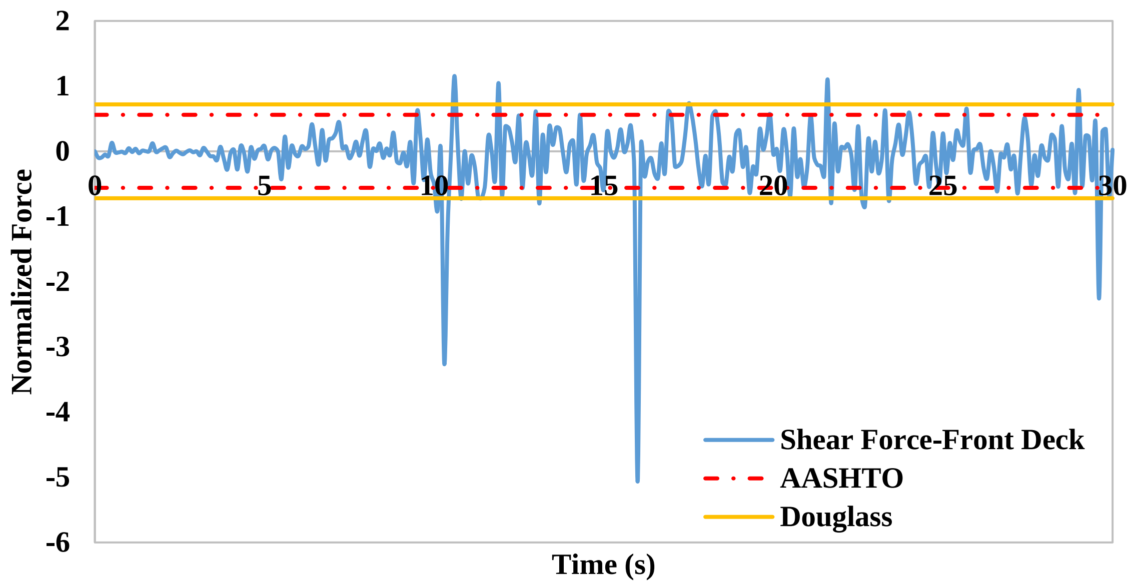

Figure 38. Shear Force-Front deck of one pier model.

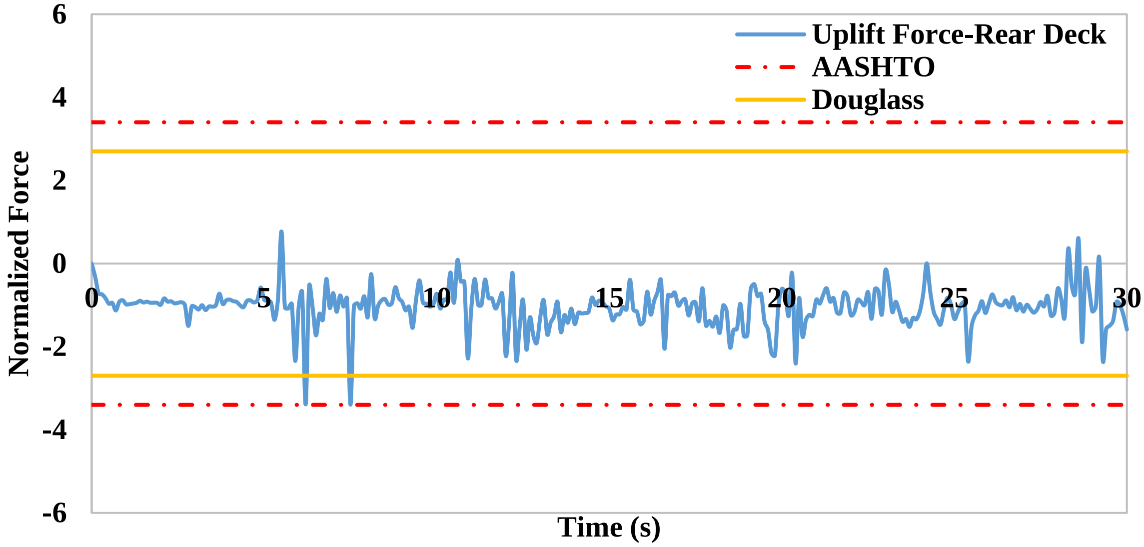

Figure 39. Uplift Force-Rear deck of one pier model.

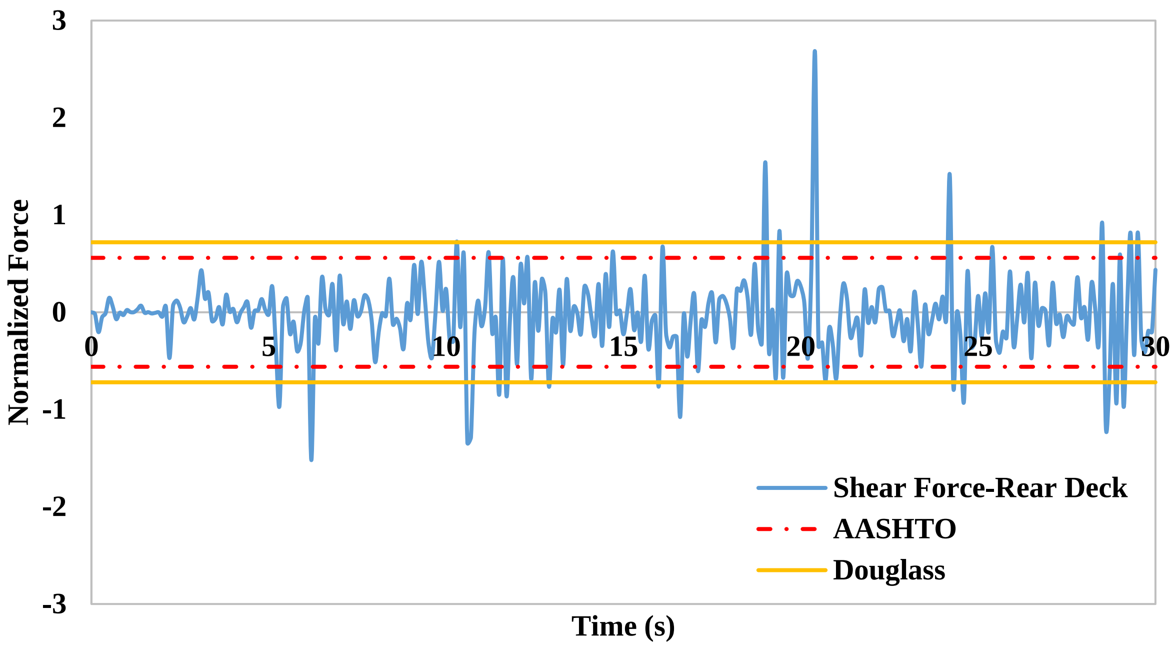

Figure 40. Uplift Force-Rear deck of one pier model.

6. CONCLUSIONS

In this research work, the response of coastal bridges with a concrete superstructure under the impact of hurricane induced waves were simulated numerically using the CEL technique within the Abaqus commercial software.

An approach for defining boundary conditions to replicate periodic waves induced during a hurricane was established. Numerical studies indicated that the desired wavelength and wave amplitude could be obtained in the CEL simulations. The discussion, insights, and general guidelines provided in this report are expected to facilitate the reproducibility of the results and promote future research work among the scientific community interested in this area.

The numerical studies revolved around two major highway bridges along the U.S Gulf Coast that were severely damaged during hurricane Katrina in 2005, (a) the U.S 90 highway bridge over Biloxi-Bay and (b) the US. 90 St. Louis-Bay Bridge. A uniqueness of the models generated in this study is that the actual dimensions of the bridge were considered in the analysis. The wave characteristics of the simulation were defined according to those expected during catastrophic hurricanes in the Gulf Coast. The superstructure configuration was shown to influence the peak magnitudes among the two studied bridges.

The FE simulation of the bridges with rigid support conditions generated sufficiently large forces to cause the collapse of the bridge superstructure. The flexibility of the foundations has a significant effect on the horizontal and vertical forces acting on the superstructure. The force demands were not proportional to the length of the piers, but they were presumably amplified when the natural period of the bridge coincided with that of the traveling waves. Natural frequency analyses should be conducted in future studies to verify this statement.

The comparison of CEL results to AASHTO equations provided a means to establish confidence on the numerical analysis, but also raised some concerns to be clarified in future research studies. Overall, the simulation's uplift and shear force estimates were in the range of AASHTO estimates but exhibited large numerical peaks that exceeded the magnitude of the AASHTO equations. These peaks coincided with the instances in which the wave impacted the superstructure, i.e., a pulse-type loading. Further work is required to determine if these peaks are numerical artifacts or a concern for connection design. As stated in other similar studies *(22)*, a full understanding of the hydrodynamic forces acting on structures can only be achieved by analyzing numerical simulation results, field measurements, and flume tests.

REFERENCES

1. Padgett J., DesRoches R., Nielson B., Yashinsky M., Kwon O.S., Burdette N., Tavera E. Bridge damage and repair costs from Hurricane Katrina. *Journal of Bridge Engineering*. 2008 Jan;13(1):6-14.

2. Matamoros, A., Testik, F., Nasouri, R. and Montoya, A. Coastal Bridges under Hurricane Stresses along the Texas and Louisiana Coast, Project No. 17STTSA02, 2018.

3. Durst, F., Miloievic, D. and Schönung, B. Eulerian and Lagrangian predictions of particulate two-phase flows: a numerical study. *Applied Mathematical Modelling*, 1984. 8(2), pp.101-115.

4. Hayatdavoodi M., Treichel K., Ertekin R.C. Parametric study of nonlinear wave loads on submerged decks in shallow water. *Journal of Fluids and Structures*, 2019. 1;86:266-89.

5. AASHTO. Guide Specifications for Bridges Vulnerable to Coastal Storms. *American Association of State Highway and Transportation Officials*, Washington, D.C, 2008.

6. Park H., Do T., Tomiczek T., Cox D.T., van de Lindt J.W. Numerical modeling of non-breaking, impulsive breaking, and broken wave interaction with elevated coastal structures: Laboratory validation and inter-model comparisons. *Ocean Engineering*, 2018. 158:78-98.

7. Saeidpour A., Chorzepa M.G., Christian J., Durham S. Probabilistic Hurricane Risk Analysis of Coastal Bridges Incorporating Extreme Wave Statistics. *Engineering Structures*, 2019. 182:379-90.

8. Yuan P., Xu G., Chen Q., Cai C.S. Framework of Practical Performance Evaluation and Concept of Interface Design for Bridge Deck–Wave Interaction. *Journal of Bridge Engineering*, 2018. 23(7):04018048.

9. He L., Attard T.L., Zhou H., Brooks A. Integrating Energy Transferability into The Connection-Detail of Coastal Bridges Using Reinforced Interfacial Epoxy-Polyurea Reaction Matrix Composite. *Composite Structures*, 2019.

10. Huang B., Zhu B., Cui S., Duan L., Zhang J. Experimental and Numerical Modelling of Wave Forces on Coastal Bridge Superstructures with Box Girders, Part I: Regular waves. *Ocean Engineering*, 2018. 149:53-77.

11. Qu K., Tang H.S., Agrawal A., Cai Y., Jiang C.B. Numerical Investigation of Hydrodynamic Load on Bridge Deck Under Joint Action of Solitary Wave and Current. *Applied Ocean Research*, 2018. 75:100-16.

12. Sheppard D.M., Dompe P.E., Gosselin M.S., Demir H. Development of Wave and Surge Atlas for The Design and Protection of Coastal Bridges in South Louisiana-Phase 2. *Louisiana Transportation Research Center*; 2016.

13. Douglass, S.L., Chen, Q., Olsen, J.M., Edge, B.L., and Brown, D. Wave Forces on Bridge Decks. *Office of Bridge Technolog16*Washington, D.C, 2006.

14. Robertson, I.N., Riggs, H.R., Yim, S.C. and Young, Y.L. Lessons from Hurricane Katrina Storm Surge on Bridges and Buildings. *Journal of Waterway, Port, Coastal, and Ocean Engineering*, 2017, *133*(6), pp.463-483.

15. R. T. P. N. O. C. Zienkiewicz, The Finite Element Method for Fluid Dynamics, 2014.

16. D. J. Benson, Computational Methods in Lagrangian and Eulerian Hydrocodes, vol. 99, *Computer Methods in Applied Mechanics and Engineering*, 1992, pp. 235-394.

17. ABAQUS, C. Analysis user's manual, 2017.

18. Dean RG, Dalrymple RA. Water Wave Mechanics for Engineers and Scientists, Prentice-Hall. Inc., Englewood Cliffs, New Jersey, 1984.

19. Lamb H. Hydrodynamics. Cambridge university press, 1993.

20. Madsen OS. On the generation of long waves. *Journal of Geophysical Research*, 1971. 76(36):8672-83.

21. Chen Q, Wang L, Zhao H. Hydrodynamic investigation of coastal bridge collapse during Hurricane Katrina. *Journal of Hydraulic Engineerin*g, 2009. 135(3):175-86.

22. Kortenhaus A, Oumeraci H, Allsop NW, McConnell KJ, Van Gelder PH, Hewson PJ, Walkden M, Müller G, Calabrese M, Vicinanza D. .1: Wave Impact Loads-Pressures and Forces. Final Proceedings, MAST III, PROVERBS-Project: Vol. IIa: *Hydrodynamic Aspects*, 1999.

APPENDIX A: US-90 BRIDGE OVER BAY ST. LOUIS DRAWINGS

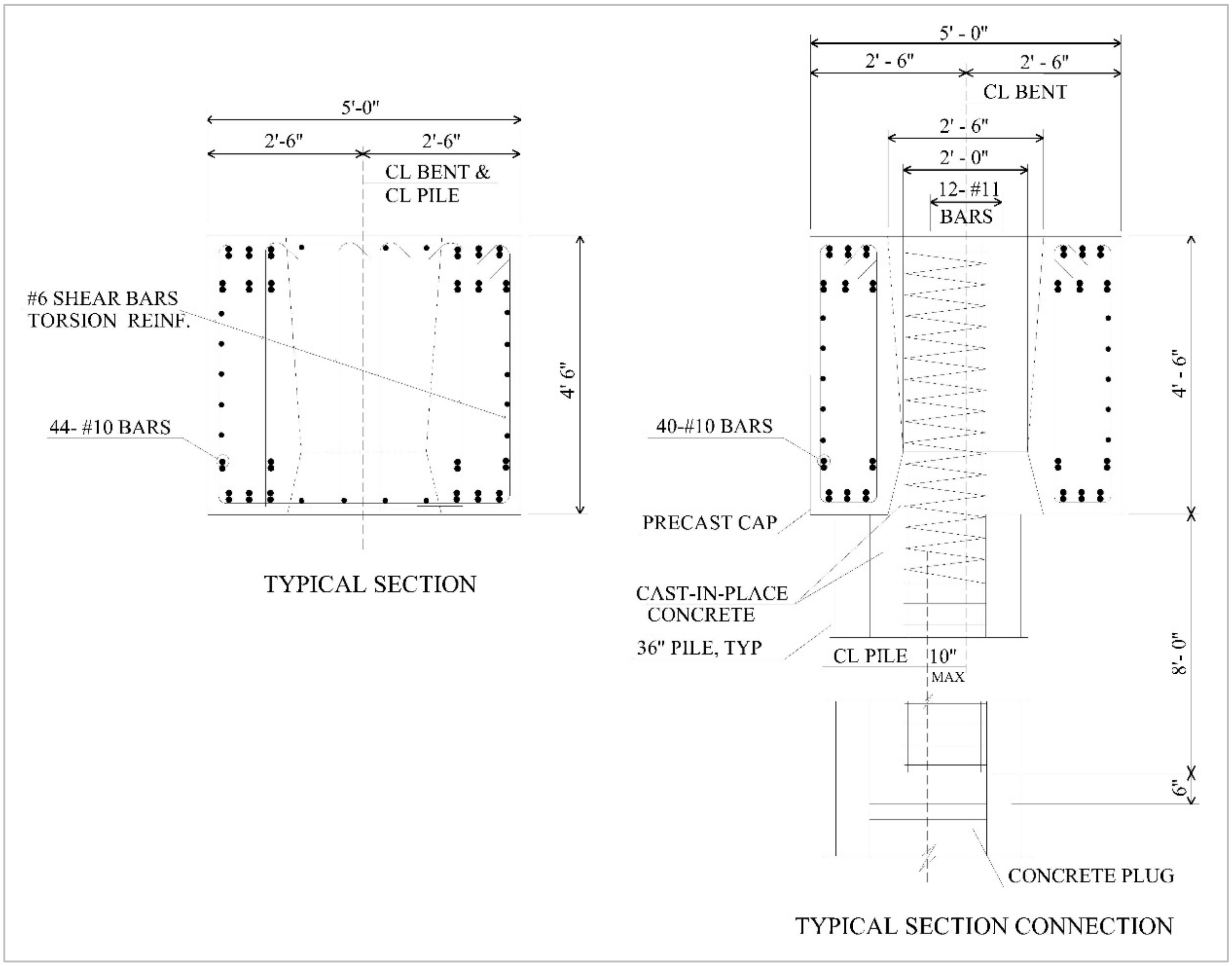

Figure A1. Cap beam to pile connection details: Typical cap beam.

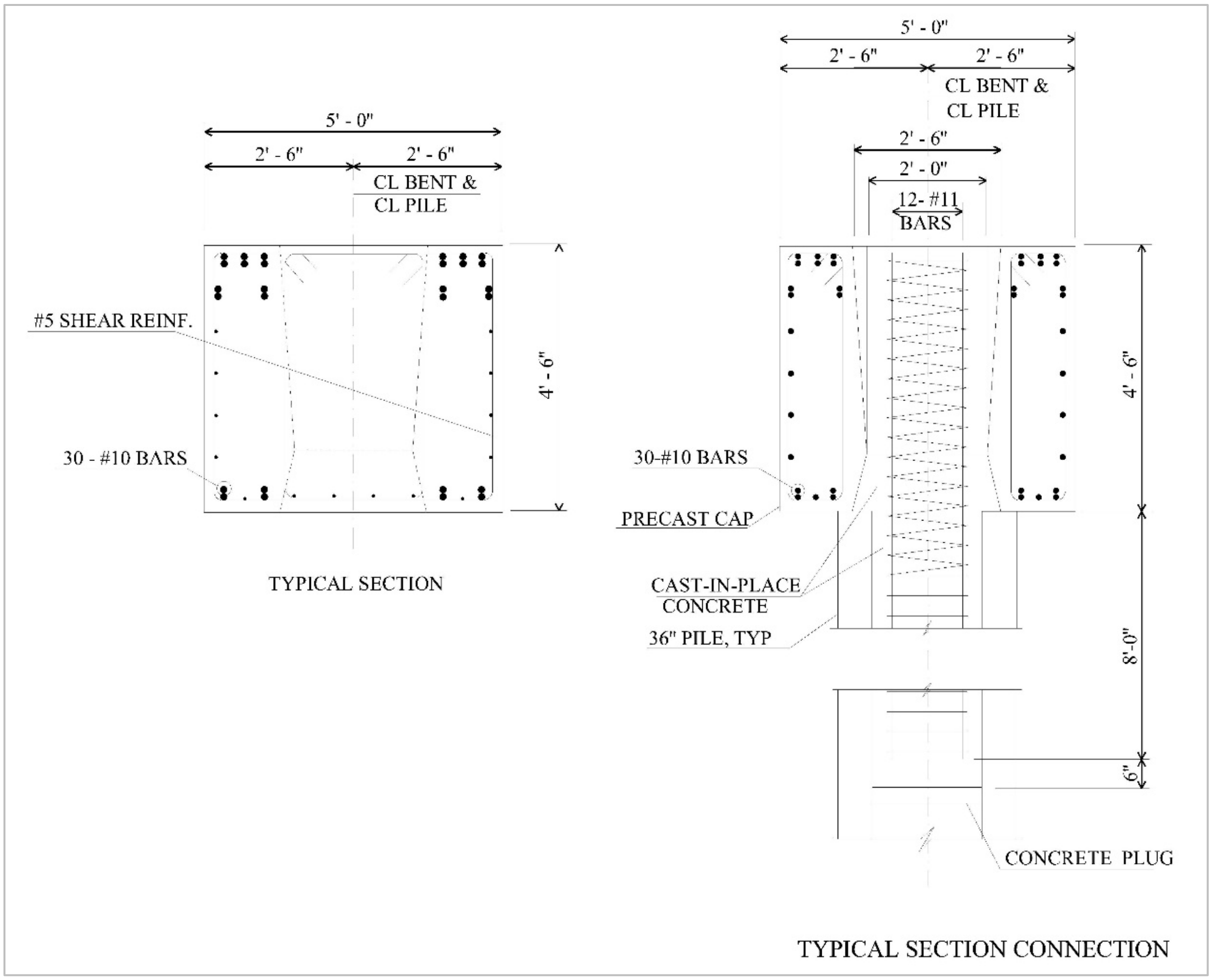

Figure A2. Cap beam to pile connection details: Enhanced torsional.

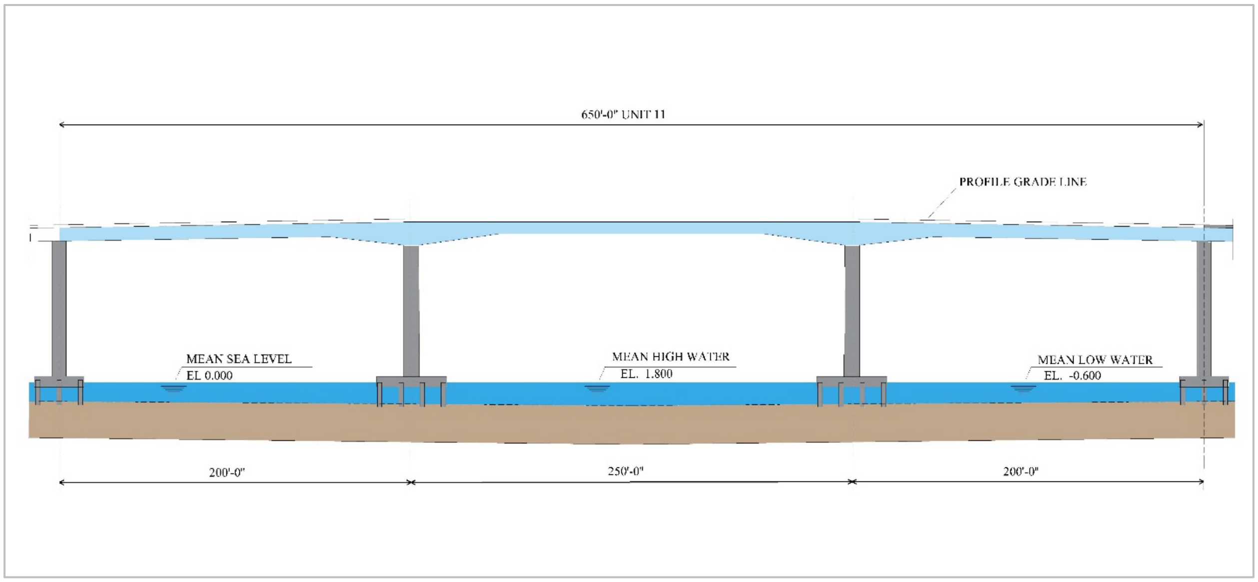

Figure A3. Bridge profile.